Article

# Counterion Controlled Photoisomerization of Retinal Chromophore Models: a Computational Investigation

Alessandro Cembran, Fernando Bernardi, Massimo Olivucci, and Marco Garavelli

*J. Am. Chem. Soc.*, **2004**, 126 (49), 16018-16037• DOI: 10.1021/ja048782+ • Publication Date (Web): 13 November 2004

J|A|C|S
ARTICLES
Published on Web 11/13/2004

# Counterion Controlled Photoisomerization of Retinal Chromophore Models: a Computational Investigation

Alessandro Cembran,[†] Fernando Bernardi,[†] Massimo Olivucci,*[,‡,§] and Marco Garavelli*[,†]

*Contribution from the Dipartimento di Chimica "G. Ciamician", Università di Bologna, via Selmi 2, Bologna, I-40126 Italy; Dipartimento di Chimica, Università di Siena, via Aldo Moro, Siena, I-53100 Italy; and Centro per lo Studio dei Sistemi Complessi, Via Tommaso Pendola 37, Siena I-53100 Italy*

Received March 3, 2004; E-mail: marco.garavelli@unibo.it

***Abstract:*** CASPT2//CASSCF photoisomerization path computations have been used to unveil the effects of an acetate counterion on the photochemistry of two retinal protonated Schiff base (PSB) models: the 2-*cis*-penta-2,4-dieniminium and the all-*trans*-epta-2,4,6-trieniminium cations. Different positions/orientations of the counterion have been investigated and related to (i) the spectral tuning and relative stability of the $S_0$, $S_1$, and $S_2$ singlet states; (ii) the selection of the photochemically relevant excited state; (iii) the control of the radiationless decay and photoisomerization rates; and, finally, (iv) the control of the photoisomerization stereospecificity. A rationale for the results is given on the basis of a simple (electrostatic) qualitative model. We show that the model readily explains the computational results providing a qualitative explanation for different aspects of the experimentally observed "environment" dependent PSB photochemistry. Electrostatic effects likely involved in controlling retinal photoisomerization stereoselectivity in the protein are also discussed under the light of these results, and clues for a stereocontrolled electrostatically driven photochemical process are presented. These computations provide a rational basis for the formulation of a mechanistic model for photoisomerization electrostatic catalysis.

## 1. Introduction

The protonated Schiff base (PSB) of retinal is the chromophore of rhodopsin proteins.[1−6] These include the retina visual pigment of animals rhodopsin (Rh), the proton and chloride pumping pigments of *Halobacterium halobium* bacteriorhodpsin (bR) and halorhodopsin (hR), respectively, and other bacterial pigments such as sensory rhodopsins (sR). The biological activity of rhodopsins is triggered by the ultrafast light-induced cis−trans isomerization of the corresponding retinal chromophores that, in turn, induces a conformational change in the protein.[1,5] This photochemical step is usually referred to as the primary event of the protein photocycle and represents one of the fastest photochemical reactions observed so far in nature (200 fs in Rh).

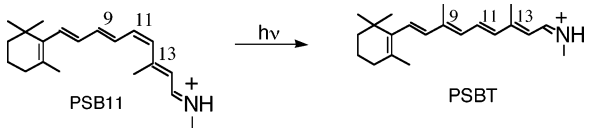


Recently, we have reported the results of a series of ab initio multiconfigurational second-order perturbation theory computations for the photoisomerization path mapping of PSB models of different chain length in isolated conditions (i.e., in vacuo). These include, among the others, the minimal PSB model 2-*cis*-penta-2,4-dieniminium cation **1**,[7] the all-*trans*-epta-2,4,6-trieniminium cation **2**,[8] and the 11-cis (PSB11) and all-trans (PSBT) retinal chromophore models 4-*cis*-$\gamma$-methylnona-2,4,6,8-tetraeniminium **3** and all-*trans*-nona-2,4,6,8-tetraeniminium **4** cations, respectively.[9−11] As reported in ref 10, photoisomerization path computations on models **1**−**4** have provided a unified and unambiguous (although qualitative) view of the *intrinsic* (i.e., absence of environmental effects) photochemical reactivity of PSBs. Despite the different length of the conjugated chain (which quantitatively affects the spectroscopy and the energetic of the system) and the lack of the retinal $\beta$-ionone ring (which could play a role in the steric factors involved in

[†] Università di Bologna.
[‡] Università di Siena.
[§] Centro per lo Studio dei Sistemi Complessi.

(1) Kandori, H.; Shichida, Y.; Yoshizawa, T. *Biochemistry (Moscow)* **2001**, *66*, 1197.
(2) Needleman, R. Bacteriorhodopsin and Rhodopsin. In *CRC Handbook of Organic Photochemistry and Photobiology*; Horspool, W. M., Song, P.-S., Eds.; CRC Press: Boca Raton, FL, 1995; pp 1508−1515.
(3) Ottolenghi, M.; Sheves, M. *Isr. J. Chem.* **1995**, *35*, U3.
(4) Wald, G. *Science* **1968**, *162*, 230.
(5) Mathies, R.; Lugtenburg, J. The Primary Photoreaction of Rhodopsin. In *Molecular Mechanism of Vision*; Stavenga, D. G., DeGrip, W. J., Pugh, E. N. J., Eds.; Elsevier Science Press: New York, 2000; Vol. 3, pp 55−90.
(6) Yoshizawa, T.; Kuwata, O. Vision: Photochemistry. In *CRC Handbook of Organic Photochemistry and Photobiology*; Horspool, W. M., Song, P.-S., Eds.; Boca Raton, FL, 1995; pp 1493−1499.
(7) Garavelli, M.; Celani, P.; Bernardi, F.; Robb, M. A.; Olivucci, M. *J. Am. Chem. Soc.* **1997**, *119*, 6891.
(8) Garavelli, M.; Bernardi, F.; Olivucci, M.; Vreven, T.; Klein, S.; Celani, P.; Robb, M. A. *Faraday Discuss.* **1998**, *110*, 51.
(9) Garavelli, M.; Vreven, T.; Celani, P.; Bernardi, F.; Robb, M. A.; Olivucci, M. *J. Am. Chem. Soc.* **1998**, *120*, 1285.
(10) Gonzalez-Luque, R.; Garavelli, M.; Bernardi, F.; Merchan, M.; Robb, M. A.; Olivucci, M. *Proc. Natl. Acad. Sci. U.S.A.* **2000**, *97*, 9379.
(11) De Vico, L.; Page, C. S.; Garavelli, M.; Bernardi, F.; Basosi, R.; Olivucci, M. *J. Am. Chem. Soc.* **2002**, *124*, 4124.


**10.1021/ja048782+ CCC: $27.50** 

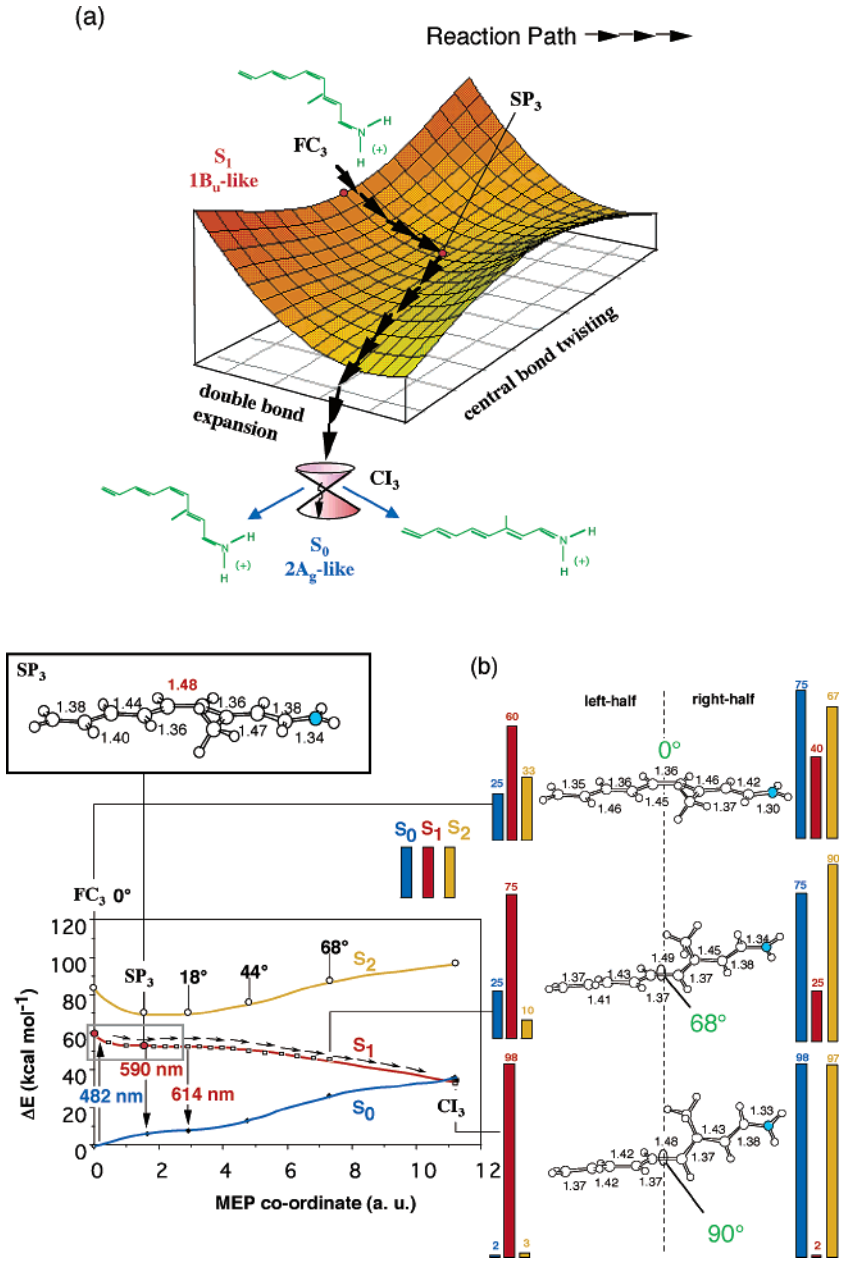


***Figure 1.*** (a) Schematic illustration of the two-mode structure of the $S_1$ ($^1B_u$-like) energy surface along the excited-state isomerization path for model **3** and (b) the corresponding computed MEP (scaled to match PT2 energy values); see ref 10. The gray frame refers to the surface reported in part a. The bar diagrams give the $S_0$, $S_1$, and $S_2$ (CAS-SCF 6-31G*) Mulliken charges for the $H_2C{=}CH{-}CH{=}CH{-}CH$ (left diagrams) and $CH{-}CH{=}CH{-}CH{=}NH_2$ (right diagrams) moieties. The stream of arrows on the $S_1$ surface represents the two-mode reaction coordinate starting at the Franck−Condon point (**FC$_3$**). Point **SP$_3$** corresponds to a flat planar stationary point on $S_1$ (i.e., a metastable species), where the torsional deformation leading to the degenerate $S_1 \rightarrow S_0$ decay funnel **CI$_3$** begins. Geometrical parameters are in Å and degrees.

constrained environments), it has been demonstrated that, in all cases, the photochemically relevant state (driving the photochemistry of the system) is the spectroscopic charge-transfer state $S_1$ (that corresponds to the $^1B_u$-like, i.e., hole-pair, spectroscopic state of polyenes). Moreover, the $S_1$ reaction coordinate along the computed barrierless photoisomerization path is curved, being sequentially dominated by two different perpendicular modes (see Figure 1a for a schematic view of the shape of the $S_1$ potential energy surface of **3**). The first mode is totally symmetric (preserving the planarity of the system) and drives the initial (<50 fs) dynamics[12] out of the Franck−Condon point (FC) through a concerted double-bond expansion and single-bond compression process involving C−C bond order inversion. The second mode is asymmetric and is dominated by the cis−trans isomerization mode that ultimately leads to a conical intersection (CI) featuring a 90° twisted central double bond (see Figure 1b). The CI features a charge-transfer electronic structure corresponding to a twisted intramolecular charge transfer (TICT) state[7,10,13] where, substantially, a "net" electron has been transferred from the "C" to the "N" end of the skeleton and, consequently the positive charge has moved from "N" to "C". Since $S_1 \rightarrow S_0$ decay at a conical intersection

(12) Ruhman, S.; Hou, B. X.; Friedman, N.; Ottolenghi, M.; Sheves, M. *J. Am. Chem. Soc.* **2002**, *124*, 8854.

(13) Garavelli, M.; Bernardi, F.; Celani, P.; Robb, M. A.; Olivucci, M. *J. Photochem. Photobiol. A: Chem.* **1998**, *114*, 109.

is fully efficient, these data provide a rationale for the ultrafast radiationless decay and the short (picosecond or subpicosecond) excited state lifetime observed in PSB chromophores. Notice that, only after the initial stretching relaxation has occurred, the $S_1$ reaction coordinate changes sharply its direction and the second out-of-plane twisting mode gets populated (see Figure 1a). The relaxed planar structure located on the $S_1$ surface (i.e., the stationary point SP where the central double bonds are fully stretched) represents the "turning point" for such a direction change and is located along a flat region whose extension depends on the length of the PSB chain.

In the past we have reported that, for model **3**,[9,10,14,15] the computed absorption and fluorescence maxima, changes in dipole moments, and simulated resonance Raman spectra are close to the corresponding experimental quantity for PSB11 both in solution and in the Rh cavity, providing a qualitative validation for the model used as well as for the force field driving the early stages of the excited-state dynamics out of the FC region.[16] Notice that the computed two-mode (i.e., first stretching then torsion) coordinate of the $S_1$ relaxation path of retinal PSB models has now been validated by different laboratories using different time-resolved spectroscopy methods[12,17−21] for retinal proteins (i.e., bR and Rh) as well as for retinal chromophores in solution.

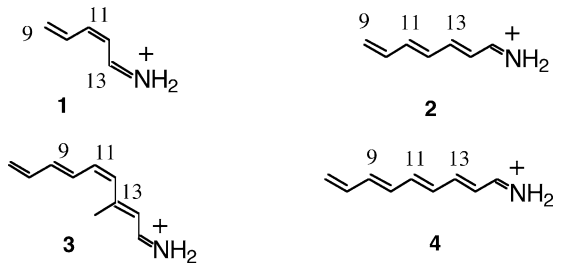


As stressed above all we know on the $S_1$ relaxation coordinate of retinal PSBs comes from computations carried out for in vacuo (i.e., isolated) chromophore models. No environment effects have ever been included in these computations. In contrast, it is experimentally known that the environment affects different aspects of the photoisomerization process such as the rate, selectivity, efficiency, and quantum yields (QYs). For instance, in Rh (bR) the excited-state PSB11 (PSBT) lifetime (following a monoexponential decay)[22] is ca. 150 fs (200fs)[23] and its photoisomerization takes place in 200 fs (500 fs)[24,25] leading to the unique all-trans PSBT (13-cis PSB13) photoproduct with a high 67% (65%) QY.[26] This behavior is different from that observed for the same chromophores in solution (methanol or hexane) where, for instance, the excited-state lifetime follows a biexponential decay[22,27] with a dominant (almost 20-fold longer) 3 ps shorter component[28] and there is a lack of stereospecificity and a decrease in the photoisomerization efficiency (to a low 25% QY).[29,30] It is thus apparent that the protein is able to "catalyze" (i.e., speed up and select) the photoisomerization with respect to the solution environment.

Among others, the intermolecular interaction of the chromophore with the counterion (usually a carboxylate anion) must play a crucial role in determining the environment effects. In fact, as mentioned above, the photochemically relevant $S_1$ state is a "hole-pair" charge transfer state.[7,9,10,13] Thus its relative energy and stability with respect to the "dot−dot" $S_2$ and $S_0$ covalent states must depend on the position of the counterion relative to the chromophore backbone. Pioneering studies and first qualitative models of counterion effects on retinal PSB photochemistry are due to Warshel,[31] Birge, Nakanishi, Honig, Sheves,[32−38] Michl, and Bonacic−Koutecky.[39,40] More recently, retinal PSB−counterion interactions have been investigated by means of solid-state NMR experiments by Smith and co-workers,[41−43] while novel theoretical analysis has been presented by Sakurai and co-workers[44,45] unveiling medium and counterion effects on the photophysical properties of the system. Similarly, environment affected vertical absorptions and spectral shifts for retinal chromophores have been recently investigated using semiempirical[46] and QM/MM[47] calculations, which revealed the importance of the interactions with nearby charged residues. Anyway, all these studies did not focus on the photoreactivity effects: the only recent ab initio mechanistic investigation on this topic is due to Nonella[48] but involves only *tight-bound* ionic pairs (i.e., the counterion is close to the nitrogen-head of the

(14) Garavelli, M.; Negri, F.; Olivucci, M. *J. Am. Chem. Soc.* **1999**, *121*, 1023.
(15) Cembran, A.; Bernardi, F.; Olivucci, M.; Garavelli, M. *J. Am. Chem. Soc.* **2003**, *125*, 12509.
(16) One possible reason for the success of model **3** is that retinal PSB11 has a highly twisted (ca. 60°) $\beta$-ionone ring both in solution (see Albeck, A.; Livnah, N.; Gottlieb, H.; Sheves, M. *J. Am. Chem. Soc.* **1992**, *114*, 2400) and in Rh (see Teller, D. C.; Okada, T.; Behnke, C. A.; Palczewski, K.; Stenkamp, R. E. *Biochemistry* **2001**, *40*, 7761−7772). This prevents efficient conjugation of the $\beta$-ionone double bond with the rest of the conjugated chain, making **3** a realistic model for retinal PSBs.
(17) Kobayashi, T.; Saito, T.; Ohtani, H. *Nature* **2001**, *414*, 531.
(18) Hou, B.; Friedman, N.; Ruhman, S.; Sheves, M.; Ottolenghi, M. *J. Phys. Chem. B* **2001**, *105*, 7042.
(19) Haran, G.; Morlino, E. A.; Matthes, J.; Callender, R. H.; Hochstrasser, R. M. *J. Phys. Chem. A* **1999**, *103*, 2202.
(20) Logunov, S. L.; Volkov, V. V.; Braun, M.; El-Sayed, M. A. *Proc. Natl. Acad. Sci. U.S.A.* **2001**, *98*, 8475.
(21) Kandori, H.; Furutani, Y.; Nishimura, S.; Shichida, Y.; Chosrowjan, H.; Shibata, Y.; Mataga, N. *Chem. Phys. Lett.* **2001**, *334*, 271.
(22) Hamm, P.; Zurek, M.; Roschinger, T.; Patzelt, H.; Oesterhelt, D.; Zinth, W. *Chem. Phys. Lett.* **1996**, *263*, 613.
(23) Kandori, H.; Sasabe, H.; Nakanishi, K.; Yoshizawa, T.; Mizukami, T.; Shichida, Y. *J. Am. Chem. Soc.* **1996**, *118*, 1002.
(24) Schoenlein, R. W.; Peteanu, L. A.; Mathies, R. A.; Shank, C. V. *Science* **1991**, *254*, 412.
(25) Mathies, R. A.; Cruz, C. H. B.; Pollard, W. T.; Shank, C. V. *Science* **1988**, *240*, 777.
(26) Dartnall, H. J. A. *Vision Res.* **1967**, *8*, 339.
(27) Logunov, S. L.; Song, L.; ElSayed, M. A. *J. Phys. Chem.* **1996**, *100*, 18586.
(28) Kandori, H.; Katsuta, Y.; Ito, M.; Sasabe, H. *J. Am. Chem. Soc.* **1995**, *117*, 2669.
(29) Becker, R. S.; Freedman, K. A. *J. Am. Chem. Soc.* **1985**, *107*, 1477.
(30) Koyama, Y.; Kubo, K.; Komori, M.; Yasuda, H.; Mukai, Y. *Photochem. Photobiol.* **1991**, *54*, 433.
(31) Weiss, R. M.; Warshel, A. *J. Am. Chem. Soc.* **1979**, *101*, 6131.
(32) Sheves, M.; Kohne, B.; Mazur, J. *Chem. Commun.* **1983**, 1232.
(33) Sheves, M.; Nakanishi, K.; Honig, B. *J. Am. Chem. Soc.* **1979**, *101*, 7086.
(34) Nakanishi, K.; Balogh-Nair, V.; Arnaboldi, M.; Tsujimoto, K.; Honig, B. *J. Am. Chem. Soc.* **1980**, *102*, 7945.
(35) Motto, M. G.; Sheves, M.; Tsujimoto, K.; Balogh-Nair, V.; Nakanishi, K. *J. Am. Chem. Soc.* **1980**, *102*, 7947.
(36) Honig, B.; Dinur, U.; Nakanishi, K.; Balogh-Nair, V.; Gawinowicz, M. A.; Arnaboldi, M.; Motto, M. G. *J. Am. Chem. Soc.* **1979**, *101*, 7084.
(37) Honig, B.; Greenberg, A. D.; Dinur, U.; Ebrey, T. G. *Biochemistry* **1976**, 4593.
(38) Birge, R. R.; Hubbard, L. M. *J. Am. Chem. Soc.* **1980**, *102*, 2195.
(39) Michl, J.; Bonacic-Koutecky, V. *Electronic aspects of organic photochemistry*; John Wiley & Sons: New York, 1990.
(40) Bonacic-Koutecky, V.; Koutecky, J.; Michl, J. *Angew. Chem., Int. Ed. Engl.* **1987**, *26*, 170.
(41) Han, M.; DeDecker, B. S.; Smith, S. O. *Biophys. J.* **1993**, *65*, 899.
(42) Han, M.; Smith, S. O. *Biochemistry* **1995**, *34*, 1425.
(43) Eilers, M.; Reeves, P. J.; Ying, W.; Khorana, H. G.; Smith, S. O. *Proc. Natl. Acad. Sci. U.S.A.* **1999**, *96*, 487.
(44) Houjou, H.; Inoue, Y.; Sakurai, M. *J. Am. Chem. Soc.* **1998**, *120*, 4459.
(45) Houjou, H.; Sakurai, M.; Inoue, Y. *Chem. Lett.* **1996**, 1075.
(46) Ren, L.; Martin, C. H.; Wise, K. J.; Gillespie, N. B.; Luecke, H.; Lanyi, J. K.; Pudich, J. L.; Birge, R. R. *Biochemistry* **2001**, *40*, 13906.
(47) Hayashi, S.; Tajkhorshid, E.; Pebay-Peyroula, E.; Royant, A.; Landau, E. M.; Navarro, J.; Schulten, K. *J. Phys. Chem. B* **2001**, *105*, 10124.
(48) Nonella, M. *J. Phys. Chem. B* **2000**, *104*, 11379.

chromophore), and to our knowledge, no detailed and systematic mechanistic information is presently available for the primary effects due to an external electrostatic field on the excited-state reactivity. The lack of accurate ab initio computations and systematic investigations of the "first-order" counterion effects on the singlet manifold structure (i.e., mainly on the $S_0$, $S_1$, $S_2$ states) and photochemical reactivity of PSBs provides the motivation for this work.

Thus, similar to previous work,[7,9,10,13,14,49] here we use the shorter retinal PSB models **1** and **2** to investigate the counterion effect on the singlet manifold ($S_0$, $S_1$, $S_2$) and, most important, on the $S_1$ relaxation path. An acetate counterion is placed at an ca. 3 Å distance as observed for analogous counterions both in the protein and in condensed phase (see also sections 2 and 4).[41−43,50−53] Notice that, in the present study, the acetate is treated at the ab initio quantum mechanical level to avoid missing important electrostatic contributions (e.g., polarizability). The counterion effect is probed for the positions/orientations defined by the structures **1a**, **1b**, **1c** and **2a**, **2b**, **2c**, **2d** (see section 4) and is investigated through the evaluation of the relative stability of the $S_0$, $S_1$, $S_2$ states and via excited-state relaxation path computations using the same ab initio CASPT2//CASSCF level of theory. When possible, the computational results are validated by comparison with the experimentally observed behavior for analogous systems (see section 6). Below we show that while these results provide information on the factors responsible for (i) the relative stability of the $S_0$, $S_1$, and $S_2$ states; (ii) the selection of the photochemically relevant excited state; (iii) the excited state lifetime and reaction rate and (iv) the control of the photoisomerization stereospecificity, a predictive and simple qualitative (electrostatic) model readily rationalizes the computational results providing an explanation for different aspects of the observed "environment" effect.

Although the energetics delivered by these shorter retinal models may be quite different than those for retinal itself, still we think we can have a qualitatively correct picture for the effects of a countercharge on the photochemistry and spectral tuning of PSBs in general, as we previously showed for PSBs in vacuo.

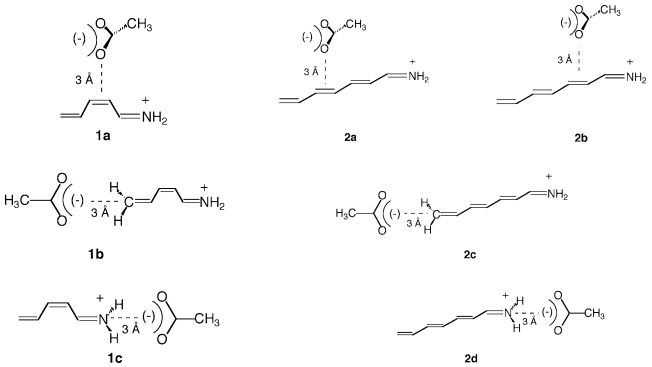


(49) Garavelli, M.; Bernardi, F.; Robb, M. A.; Olivucci, M. *J. Mol. Struct.* **1999**, *463*, 59.
(50) Elia, G. R.; Childs, R. F.; Britten, J. F.; Yang, D. S. C.; Santarsiero, B. D. *Can. J. Chem.* **1996**, *74*, 591.
(51) Choi, C. S.; Prask, H. J.; Prince, E. *J. Chem. Phys.* **1974**, *61*, 3523.
(52) Palczewski, K.; Kumasaka, T.; Hori, T.; Behnke, C. A.; Motoshima, H.; Fox, B. A.; Le Trong, I.; Teller, D. C.; Okada, T.; Stenkamp, R. E.; Yamamoto, M.; Miyano, M. *Science* **2000**, *289*, 739.
(53) Childs, R. F.; Shaw, G. S.; Wasylishen, E. *J. Am. Chem. Soc.* **1987**, *109*, 5362.

## 2. Computational Details

The FC→CI or FC→TM (i.e., twisted minimum) excited-state reaction coordinates for models with (**1a**, **1b**, **1c** and **2a**, **2b**, **2c**, **2d**) and without (**1** and **2**) the external counterion have been obtained via reaction path computations and geometry optimizations carried out at the CASPT2//CASSCF/6-31G* level. (The reaction coordinate is computed at the CASSCF level of theory, while the associated energy profile is evaluated via single-point CASPT2[54] computations on a selected number of points along the path or/and relevant stationary points by using the method included in MOLCAS-5.[55] Unless differently stated, the zeroth order wave functions used in the CASPT2 calculations are three root ($S_0$, $S_1$, and $S_2$) state average CASSCF (the $\pi$ 8e/8o for **2**, **2a**, **2b**, **2c**, **2d**) wave functions. The *core* orbitals have always been kept frozen.)

The selected CAS active space comprises the full $\pi$-system *of the PSB*. On the other hand, the full set of acetate anion orbitals are enclosed in the core and virtual space. A preliminary calibration analysis performed by comparing calculations with a diffuse functions expanded basis set (6-31+G*) has shown that no appreciable differences exist on both the energetics and the force field, justifying the use of the less demanding 6-31G* basis set. The single-state CASSCF computations have been used for excited states when possible, while a state average procedure between two ($S_0$, $S_1$) or three ($S_0$, $S_1$, $S_2$) roots has been used (with identical weights) in all other cases to avoid CASSCF convergence problems (see tables for the details).

Excited-state reaction computations are determined in terms of minimum energy paths (MEP) in mass-weighted coordinates using the full set of vibrational degrees of freedom of the molecule. MEP computations have been performed using the prescriptions reported in refs 56 and 57 (see also Supporting Information for further details). In the past, this strategy has been successfully applied to the investigation of the photochemistry of neutral conjugated hydrocarbons[58−64] and PSBs.[7,9,10,13,14,49] The use of MEP for the interpretation of the observed excited-state dynamics of short PSBs has been validated via semiclassical trajectory computations.[65−67] The reaction coordinate is reported in mass-weighted atomic units (au). All these computations have been carried out with the GAUSSIAN98 series of programs.[68]

The details of the geometrical arrangement and constraints used to anchor the position of the acetate relative to the chromophore are reported in the Appendix and in the Supporting Information. These anchoring points are used to avoid the anion/cation collapse. In all cases, the shortest distance between the counterion and the PSB chromophore has been fixed to 3 Å consistently with the experimental observations in the protein matrix, in solution, and in crystals.[41−43,50−53]

(54) Andersson, K.; Malmqvist, P. A.; Roos, B. O. *J. Chem. Phys.* **1992**, *96*, 1218.
(55) Andersson, K.; Blomberg, M. R. A.; Fülscher, M. P.; Karlström, G.; Lindh, R.; Malmqvist, P.-Å.; Neogrády, P.; Olsen, J.; Roos, B. O.; Sadlej, A. J.; Schütz, M.; Seijo, L.; Serrano-Andrés, L.; Siegbahn, P. E. M.; Widmark, P.-O. *MOLCAS*, 5.0; Lund University: Lund, 1999.
(56) Bearpark, M. J.; Robb, M. A.; Schlegel, H. B. *Chem. Phys. Lett.* **1994**, *223*, 269.
(57) Celani, P.; Robb, M. A.; Garavelli, M.; Bernardi, F.; Olivucci, M. *Chem. Phys. Lett.* **1995**, *243*, 1.
(58) Garavelli, M.; Bernardi, F.; Cembran, A.; Castano, O.; Frutos, L. M.; Merchan, M.; Olivucci, M. *J. Am. Chem. Soc.* **2002**, *124*, 13770.
(59) Garavelli, M.; Bernardi, F.; Moliner, V.; Olivucci, M. *Angew. Chem., Int. Ed.* **2001**, *40*, 1466.
(60) Garavelli, M.; Celani, P.; Bernardi, F.; Robb, M. A.; Olivucci, M. *J. Am. Chem. Soc.* **1997**, *119*, 11487.
(61) Fuss, W.; Haas, Y.; Zilberg, S. *Chem. Phys.* **2000**, *259*, 273.
(62) Garavelli, M.; Frabboni, B.; Fato, M.; Celani, P.; Bernardi, F.; Robb, M. A.; Olivucci, M. *J. Am. Chem. Soc.* **1999**, *121*, 1537.
(63) Garavelli, M.; Page, C. S.; Celani, P.; Olivucci, M.; Schmid, W. E.; Trushin, S. A.; Fuss, W. *J. Phys. Chem. A* **2001**, *105*, 4458.
(64) Garavelli, M.; Smith, B. R.; Bearpark, M. J.; Bernardi, F.; Olivucci, M.; Robb, M. A. *J. Am. Chem. Soc.* **2000**, *122*, 5568.
(65) Vreven, T.; Bernardi, F.; Garavelli, M.; Olivucci, M.; Robb, M. A.; Schlegel, H. B. *J. Am. Chem. Soc.* **1997**, *119*, 12687.
(66) Garavelli, M.; Bernardi, F.; Olivucci, M.; Bearpark, M. J.; Klein, S.; Robb, M. A. *J. Phys. Chem. A* **2001**, *105*, 11496.
(67) Garavelli, M.; Celani, P.; Fato, M.; Bearpark, M. J.; Smith, B. R.; Olivucci, M.; Robb, M. A. *J. Phys. Chem. A* **1997**, *101*, 2023.

*Scheme 1*

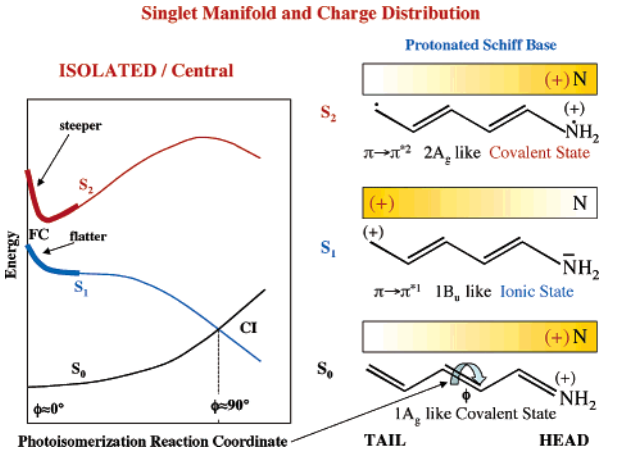


Given the general flatness of the $S_1$ energy profile along most of the computed excited state reaction paths, it is not always technically feasible to locate a transition structure (TS). In this case, optimized surface scans complemented by MEP computations starting at FC[57,67] have been used for locating the $S_1$ relaxation channels. Furthermore, even when TS optimization is possible, the energy profile recomputed at the CASPT2 level often shows a shifted energy maximum. Thus, throughout the paper the position of the $S_1$ TS and of the associated barrier is evaluated at the CASPT2 level in terms of the energy difference between the energy profile maximum and the SP intermediate.

The charge distribution (Mulliken charges) along the PSB backbone is determined at the CASSCF level of theory. In a previous paper[7] we demonstrated that, for model **1**, the atomic charges computed using different schemes (NPA, CHelpG, MKS) yield the same distribution. Similarly the computed *total* natural bond orbital (NBO)[69] charges give, again, the same type of distribution. Therefore, we think that Mulliken population analysis provides reliable results for the system investigated here as well. Mulliken charge distributions and dipole moments have been used to elucidate the nature (ionic vs covalent) of the excited singlet states involved in the photoisomerization processes.

### 3. Rationalization of the Counterion Effect

In this section we define a qualitative model for the prediction/rationalization of the counterion effect in PSB excited states. The model will be used in section 4 for the discussion and interpretation of the computational results.

**3.1. A Qualitative Electrostatic Model.** In Scheme 1 we report the structure of the singlet manifold along the computed $S_1$ reaction path for a PSB (here the penta-2,4-dieniminium cation has been used as a model).[7,9,10] In the same scheme we also provide information on the electronic nature of the singlet ($S_0$, $S_1$, $S_2$) states. Accordingly, horizontal smoothed colored bars (representing the PSB skeleton) illustrate the positive charge distribution as a function of the color intensity. Note that the initial steepness of the singlet excited states is higher for the covalent state $S_2$ (see also Figure 1b).[61,70]

*Scheme 2*

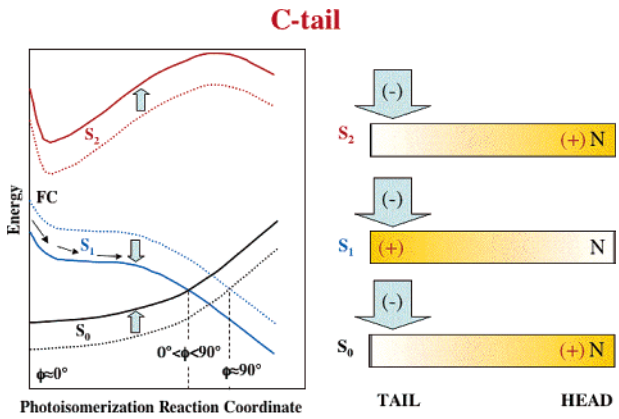


If one places a counterion close to the chromophore, its electrostatic field will stabilize the singlet ($S_0$, $S_1$, $S_2$) states depending on the distance between the negative (counterion) and the positive (chromophore) charge centers. On the other hand the position of the positive charge along the PSB backbone depends on the nature of the electronic state (e.g., it is closer to the nitrogen-head (**N-head**) for covalent states and to the carbon-tail (**C-tail**) for the charge-transfer state). Thus, opposite counterion effects are expected for different states. Indeed, three different limiting cases can be envisioned:

(a) the counterion is placed in a **Central** position above the chromophore backbone (**1a**, **2a**, **2b**). In this case the stabilization effect must be almost independent from the singlet state nature (i.e., the distance between the negative and positive charges is similar for covalent and charge-transfer states). Therefore, the structure of the singlet manifold is likely to remain substantially unchanged (see Scheme 1).

(b) the counterion is placed closer to the **C-tail** (**1b**, **2c**). In this position (see Scheme 2) the charge-transfer ($S_1$) state is stabilized (i.e., shorter couterion/positive-charge distance) with respect to the ($S_0$, $S_2$) covalent states. This leads to a change in the structure of the singlet manifold where the $S_1-S_0$ energy gap decreases and the $S_2-S_1$ increases. Consequently (according to the intensity of this effect and the slopes of the $S_1$ and $S_0$ surfaces) the $S_1/S_0$ crossing should occur earlier along the $S_1$ isomerization path.

(c) the counterion is placed closer to the **N-head** (**1c**, **2d**). In this position the covalent states ($S_0$, $S_2$) is stabilized with respect to the ($S_1$) charge-transfer state (see Scheme 3). This leads to an $S_1-S_0$ energy gap increase and an $S_2-S_1$ decrease. While the $S_1/S_0$ conical intersection is expected to occur later along the $S_1$ isomerization path, an $S_2/S_1$ crossing could be generated in this case as found in neutral polyenes[8,60−64,66,67,71−74] with a consequent change in the electronic structure of $S_1$ along the initial part of the path. Thus, while a diradical-type $S_1$ minimum could exist, an avoided crossing TS could emerge (due to a second $S_2/S_1$ crossing between the bonding covalent and antibonding ionic surfaces) along the isomerization path (see Scheme 3), which recovers the ionic (charge-transfer) nature of the $S_1$ state.

The counterion can also affect the slope of the $S_1$ isomerization path. In fact, according to previous computations,[7,9,10,39,40,75]

(68) Frisch, M. J.; Trucks, G. W.; Schlegel, H. B.; Scuseria, G. E.; Robb, M. A.; Cheeseman, J. R.; Zakrzewski, V. G.; Montgomery, J. A., Jr.; Stratmann, R. E.; Burant, J. C.; Dapprich, S.; Millam, J. M.; Daniels, A. D.; Kudin, K. N.; Strain, M. C.; Farkas, O.; Tomasi, J.; Barone, V.; Cossi, M.; Cammi, R.; Menucci, B.; Pomelli, C.; Adamo, C.; Clifford, S.; Ochterski, J.; Petersson, G. A.; Ayala, P. Y.; Cui, Q.; Morokuma, K.; Malick, D. K.; Rabuck, A. D.; Raghavachari, K.; Foresman, J. B.; Cioslowski, J.; Ortiz, J. V.; Stefanov, B. B.; Liu, G.; Liashenko, A.; Piskorz, P.; Komaromi, I.; Gomperts, R.; Martin, R. L.; Fox, D. J.; Keith, T.; Al-Laham, M. A.; Peng, C. Y.; Nanayakkara, A.; Gonzalez, C.; Challacombe, M.; Gill, P. M. W.; Johnson, B. G.; Chen, W.; Wong, M. W.; Andres, J. L.; Gonzalez, C.; Head-Gordon, M.; Replogle, E. S.; Pople, J. A. *Gaussian 98*, revision A.6; Gaussian Inc.: Pittsburgh, PA, 1998.
(69) Reed, A. E.; Curtiss, L. A.; Weinhold, F. *Chem. Rev.* **1988**, *88*, 899.
(70) There is general agreement of all multireference methods that the covalent state energy is reduced much faster during geometrical relaxation: (a) Strodel, P.; Tavan, P. *J. Chem. Phys.* **2002**, *117*, 4677. (b) Nakayama, K.; Nakano, H.; Hirao, K. *Int. J. Quantum Chem.* **1998**, *66*, 157.

***Scheme 3***

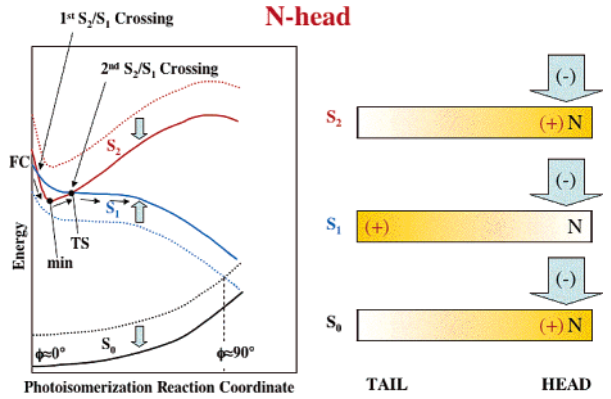


only a partial (~60%) positive charge shift from **N-head** to **C-tail** occurs upon vertical excitation. The remaining 40% charge migrates to the **C-tail** only upon isomerization (i.e., double-bond twisting), and it is completed at the twisted ($S_1/S_0$ conical intersection) point. This means that, for $S_1$, the magnitude of the counterion stabilization/destabilization increases along the path. Accordingly, we can predict a counterion effect that is smaller at FC but higher at the twisted point resulting in a decrease or increase of the slope depending on the **N-head** or **C-tail** position of the counterion, respectively (see Scheme 4). Notice that, because of these effects, an $S_1$ energy minimum and transition structure can be created in the **N-head** case. In contrast, an even earlier $S_1/S_0$ crossing is expected in the **C-tail** case.

Finally, it is worth saying that, quantitatively, the counterion effect on the singlet manifold depends on both its distance from the chromophore and the type of anion involved.[32,44,45,50] Thus, it becomes crucial to computationally evaluate these effects properly, which will be the subject of section 4. Still, we will see that our qualitative model provides the basis for the rationalization of the results.

**3.2. Conical Intersections vs Twisted Excited-State Intermediates.** In Table 1 and Figure 2 we collect the energies and geometries of the charge-transfer $S_1$ structures found for the isolated chromophores **1** and **2**. It is apparent that while the isomerization of the internal double bonds leads to a topographically *peaked*[74,76,77] $S_1/S_0$ conical intersection (the same behavior has been reported for the longer PSBs **3** and **4**),[7−10] the torsional deformation of the two terminal double bonds $CH_2$═CH− and −CH═$NH_2^+$ leads to real $S_1$ twisted minima (TM).[7] However, while the $CH_2$═CH− minima is found to correspond to a true

***Table 1.*** CASSCF/6-31g* Absolute and CASPT2/6-31G* Absolute and Relative Three-Root State Average Energies (Equal Weights Have Been Used for $S_0$, $S_1$, and $S_2$); the Weight ($\omega$) of the Zeroth Order CASSCF Wave Function in the CASPT2 Wave Function is also Reported

| structure[a] | state | CASSCF[a] (au) | CASPT2 (au) | $\omega$ | $\Delta E$ eV (kcal mol$^{-1}$) |
|---|---|---|---|---|---|
| | | Model 1 | | | |
| $FC_1$ | $S_0$ | −248.249 11 | −248.974 81 | 0.81 | 0.00 (0.00) |
| | $S_1$ | −248.069 44 | −248.829 49 | 0.78 | 3.95 (91.2) |
| | $S_2$ | −248.031 62 | −248.778 06 | 0.79 | 5.35 (123.5) |
| $SP_1$ | $S_0$ | −248.221 27 | −248.954 72 | 0.80 | 0.55 (12.6) |
| | $S_1$ | −248.081 19 | −248.839 46 | 0.78 | 3.68 (84.9) |
| | $S_2$ | −248.052 51 | −248.801 34 | 0.79 | 4.72 (108.9) |
| $TM2_1$ | $S_0$ | −248.151 61 | −248.885 32 | 0.80 | 2.44 (56.2) |
| | $S_1$ | −248.076 72 | −248.838 88 | 0.79 | 3.70 (85.3) |
| | $S_2$ | −248.046 07 | −248.791 28 | 0.69 | 4.99 (115.2) |
| $CI_1$ | $S_0$ | −248.130 45 | −248.889 09 | 0.79 | 2.33 (53.8) |
| | $S_1$ | −248.158 03 | −248.887 28 | 0.80 | 2.38 (54.9) |
| | $S_2$ | −248.037 19 | −248.766 10 | 0.78 | 5.68 (131.0) |
| $TM1_1$ | $S_0$ | −248.140 46 | −248.901 88 | 0.79 | 1.98 (45.8) |
| | $S_1$ | −248.119 56 | −248.850 88 | 0.78 | 3.37 (77.8) |
| | $S_2$ | −248.019 27 | −248.757 01 | 0.70 | 5.93 (136.7) |
| | | Model 2 | | | |
| $FC_2$ | $S_0$ | −325.174 91 | −326.129 48 | 0.76 | 0.00 (0.0) |
| | $S_1$ | −325.023 96 | −326.010 68 | 0.74 | 3.23 (74.5) |
| | $S_2$ | −324.993 01 | −325.969 71 | 0.74 | 4.35 (100.3) |
| $SP_2$ | $S_0$ | −325.148 64 | −326.112 88 | 0.75 | 0.45 (10.4) |
| | $S_1$ | −325.040 71 | −326.021 57 | 0.74 | 2.94 (67.7) |
| | $S_2$ | −325.005 90 | −325.984 46 | 0.74 | 3.95 (91.0) |
| $TM2_2$ | $S_0$ | −325.079 24 | −326.046 72 | 0.75 | 2.25 (51.9) |
| | $S_1$ | −325.001 75 | −325.990 52 | 0.74 | 3.78 (87.2) |
| | $S_2$ | −324.995 58 | −325.973 91 | 0.72 | 4.23 (97.6) |
| $CI2_2$ | $S_0$ | −325.088 76 | −326.052 78 | 0.75 | 2.09 (48.1) |
| | $S_1$ | −325.057 96 | −326.043 59 | 0.74 | 2.34 (53.9) |
| | $S_2$ | −324.982 39 | −325.953 90 | 0.73 | 4.78 (110.2) |
| $CI1_2$ | $S_0$ | −325.070 80 | −326.059 13 | 0.74 | 1.91 (44.1) |
| | $S_1$ | −325.090 51 | −326.046 13 | 0.75 | 2.27 (52.3) |
| | $S_2$ | −324.991 53 | −325.952 21 | 0.73 | 4.82 (111.2) |
| $TM1_2$ | $S_0$ | −325.103 31 | −326.068 17 | 0.75 | 1.67 (38.5) |
| | $S_1$ | −325.016 99 | −326.008 94 | 0.59 | 3.28 (75.6) |
| | $S_2$ | −324.968 39 | −325.954 07 | 0.74 | 4.77 (110.1) |

[a] All the FC and SP structures have been obtained via single-root CASSCF optimizations, while two-root state average CASSCF computations ($S_0$ and $S_1$ have been equally weighted) have been used for all the other structures reported (CASSCF energies not given).

***Scheme 4***

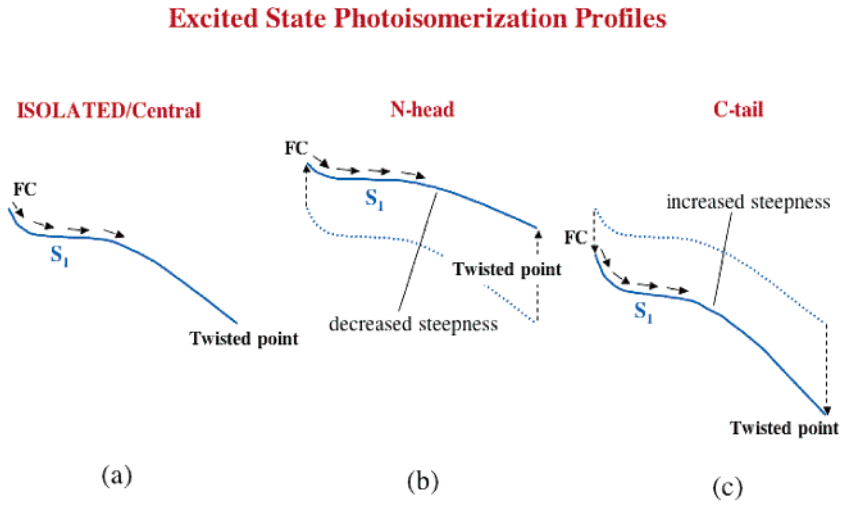

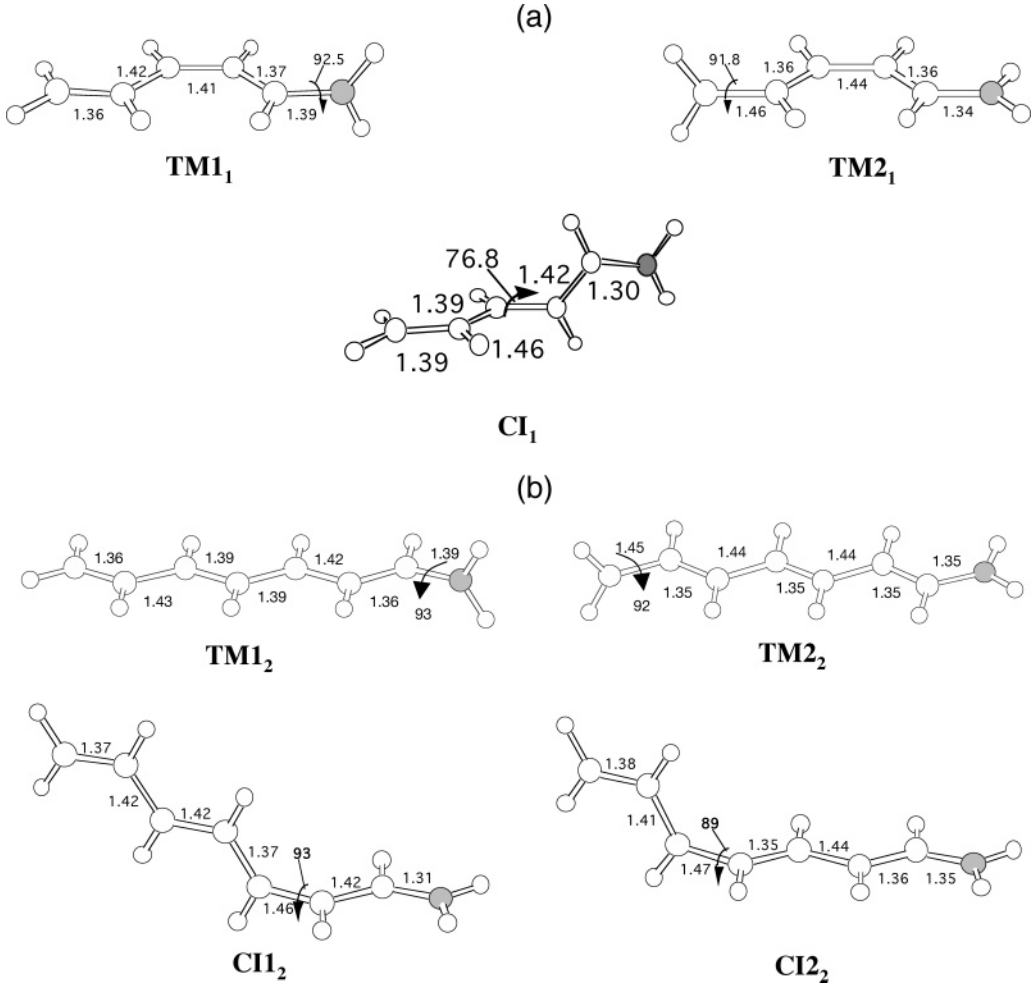


***Figure 2.*** Geometries of the twisted structures (i.e., conical intersections and twisted minima) found at the bottom of the $S_1$ surface for (a) the isolated model **1** and (b) the isolated model **2** (geometrical parameters in Å and degrees).

TICT state (i.e., the electronic structure is the same seen for the conical intersection), the $-CH=NH_2^+$ minimum has a covalent electronic structure.

The effect of the position of the counterion on the $S_1-S_0$ energy gap at these $S_1$ twisted points can be easily predicted using simple potential energy curve models for the charge-transfer (red) and covalent (blue) states (see Scheme 5). In Scheme 5a we report, for an isolated PSB, such model curves for the three (i−iii) cases defined above. Similarly, in Scheme 5b and c we report the predicted counterion effects for the **N-head** and **C-tail** positions, respectively (again, the **Central** position should leave the curves substantially unmodified; see Scheme 5a). While a relative, electrostatic stabilization of the charge-transfer curve is predicted for the **C-tail** orientation, the **N-head** orientation should result in a relative destabilization of the same curve. Accordingly, the $S_1/S_0$ crossing is predicted to shift to higher (or to lower) energies leading to a change in conical intersection topography from *peaked* to *sloped*[74,76,77] (or from *sloped* to *peaked*). Most importantly, such change may lead to the emergence of a twisted minimum (TM) replacing the *peaked* CI at the bottom of the $S_1$ energy surface. On the other hand, when the twisted double bond gets closer to the counterion (e.g., $CH_2=CH-$ for the **C-tail** and $-CH=NH_2^+$ for the **N-head** positions), the $S_1-S_0$ energy gap gets smaller, and when the magnitude of the effect is large enough, a *peaked* CI should replace the TM structure. As we will see below, such behavior will be important to provide a rationale for the computational results discussed below.

## 4. Results and Discussion

We use models **1a**, **1b**, **1c** and **2a**, **2b**, **2c**, **2d** to provide a quantitative evaluation of the counterion effects illustrated in Schemes 1−5 for the **Central**, **C-tail**, and **N-head** cases. Anyway, the shorter models (**1a**, **1b**, **1c**) lead to similar results than the longer ones (**2a**, **2b**, **2c**, **2d**). In addition, the larger systems allow us to investigate counterion effects on the photoisomerization stereoselectivity (i.e., the two internal double bonds are involved in competing photoisomerization channels). Therefore, for simplicity reasons, only the results for the longer PSB will be extensively documented and discussed here, while

(71) Hudson, B. S.; Kohler, B. E.; Schulten, K. Linear Polyene Electronic Structure and Potential Surfaces. *Excited States*; Academic Press: New York, 1982; Vol. 6, pp 1−99.
(72) Klessinger, M.; Michl, J. *Excited States and Photochemistry of Organic Molecules*; VCH: New York, 1995.
(73) Celani, P.; Garavelli, M.; Ottani, S.; Bernardi, F.; Robb, M. A.; Olivucci, M. *J. Am. Chem. Soc.* **1995**, *117*, 11584.
(74) Robb, M. A.; Garavelli, M.; Olivucci, M.; Bernardi, F. *Rev. Comput. Chem.* **2000**, *15*, 87.
(75) Garavelli, M.; Bernardi, F.; Roob, M. A.; Olivucci, M. *Int. J. Photoenergy* **2002**, *4*, 57.
(76) Bernardi, F.; Olivucci, M.; Robb, M. A. *Chem. Soc. Rev.* **1996**, *25*, 321.
(77) Atchity, G. J.; Xantheas, S. S.; Ruedenberg, K. *J. Chem. Phys.* **1991**, *95*, 1862.

***Scheme 5***

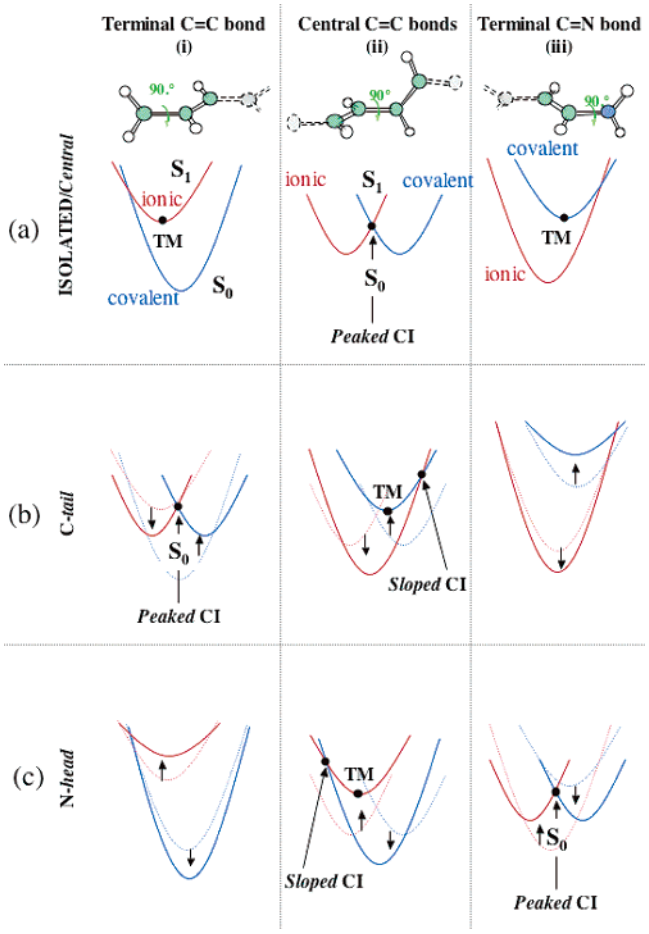


the corresponding results for **1a**, **1b**, **1c** are reported in detail only in the Supporting Information.

**4.1. Central Position.** Previous computations for **2** in vacuo[8,10] revealed the existence of two competitive $S_1$ isomerization paths of the two internal C═C double bonds (see Figure 3). For both bonds the $S_1$ paths maintain a charge-transfer character that assumes the final form of a TICT state at the corresponding $S_1/S_0$ conical intersections (**CI1**$_2$ and **CI2**$_2$). Here these paths have been reinvestigated for systems including a **Central** acetate counterion in two different positions: in **2a** the counterion is placed right above the internal C4═C5 double bond, while in **2b** the counterion is placed above the C2═C3 internal double bond. The results are reported in Figures 4 and 5, respectively.

It is apparent that, in both **2a** and **2b**, one finds the following:

(i) a barrierless $S_1$ isomerization path leading to a TICT $S_1/S_0$ CI (**CI**$_{2a}$ and **CI**$_{2b}$) still exists and corresponds to *rotation about the double bond closer to the acetate moiety* (see Figures 4 and 5);

(ii) in contrast, the isomerization paths corresponding to the alternative internal double bond are found to be less favored due to the absence of $S_1/S_0$ CIs (which have been replaced by twisted minima) and, for case **2a**, the presence of an energy barrier (see **TS**$_{2a}$ in Figure 4).

Indeed, the fact that the counterion does not remove the barrierless path and the twisted $S_1/S_0$ CI relative to the double bond closer to it (as also seen for model **1a**: see the Supporting Information Section) can be explained with the effects discussed in Scheme 6: structural analysis reveals that the distance between the positive and negative charges is more or less the same for the $S_0$ and $S_2$ covalent and the $S_1$ ionic states suggesting an "isolated-like" situation (consistent with Scheme 6a and c) which in fact preserves unchanged the isomerization path seen for the isolated system (see also Schemes 1, 4a, and 5a). On the other hand, isomerization of the internal double bond far from the counterion is unfavored due to an unbalanced stabilization of the **N-head** and **C-tail** charges in the different states. Indeed for **2a** the mean distance between the acetate and the left twisted **C-tail** fragment is significantly shorter than the one with the **N-head** moiety (see Scheme 6b), and thus the covalent state (with the $S_1$ positive charge located on the **N-head** fragment) gets less stabilized than the charge-transfer state (with the $S_1$ positive charge located on the **C-tail** fragment). For this reason the conical intersection found in vacuo when the bond is fully twisted is lost and replaced (see Scheme 5b(ii)) by a covalent minimum (**TM**$_{2a}$), as shown in Figure 4b. An opposite effect is seen for **2b** where the distance between the acetate and the twisted **C-tail** fragment is significantly larger than the one with the **N-head** (see Scheme 6d). Here, covalent states (with the positive charge located on the **N-head** fragment) become more stabilized than the charge-transfer state. Thus, according to Scheme 5c(ii), the conical intersection is removed and replaced by a TICT state minimum (**TM**$_{2b}$), as shown in Figure 5b.

The above reasoning is reinforced by the analysis of the charge distribution along the isomerization path. In fact, while the barrierless isomerization channel of **2a** (see Figure 4) maintains a charge-transfer nature all along $S_1$ (as found for the isolated chromophore), the favored but less steep path of **2b** involves *two consecutive $S_2/S_1$ avoided crossings* between the original $S_1$ charge-transfer state and the excited covalent state $S_2$ as depicted in the top part of Figure 5. Indeed, immediately after leaving the FC region on $S_1$, a first avoided crossing occurs (i.e., the $S_1$ and $S_2$ charge distribution lines cross) which changes $S_1$ into a covalent state and yield a planar diradical relaxed structure (**SP**$_{2b}$). (In contrast the relaxed planar structure found in **2a** (**SP**$_{2a}$) has a charge-transfer character.)[78]

Only at about −101° twisting (≈8.0 au) a second (avoided) crossing occurs (see the second charge distribution line crossing in the top part of Figure 5a) and restores the original charge-transfer nature of $S_1$. After this point the steepness of the path increases sharply, due to the antibonding character of the ionic state, leading to **CI**$_{2b}$. Analogous features have been observed along the alternative and less favored path reported in Figure 5b, although in this case the path enters a charge-transfer region leading to a TICT minimum (**TM**$_{2b}$). Here, a significant $S_1-S_0$ energy separation (∼20 kcal/mol) exists, and although the minimum can be easily populated along the barrierless path, radiationless decay will be strongly delayed, with a resulting decrease in isomerization rate and efficiency. Therefore, we can think to this path as a *locked* isomerization channel (or at least much less favored than the other). The same occurs for the isomerization channel reported in Figure 4b, where even an energy barrier (**TS**$_{2a}$) exists.

(78) Strictly speaking, **SP**$_{2a}$ and **SP**$_{2b}$ are not stationary points but are optimized points along the MEPs (at about 1.5 au distance from the FC point), whose gradient is small. Therefore, we assimilated this structure to the planar $S_1$ skeletal relaxed species.

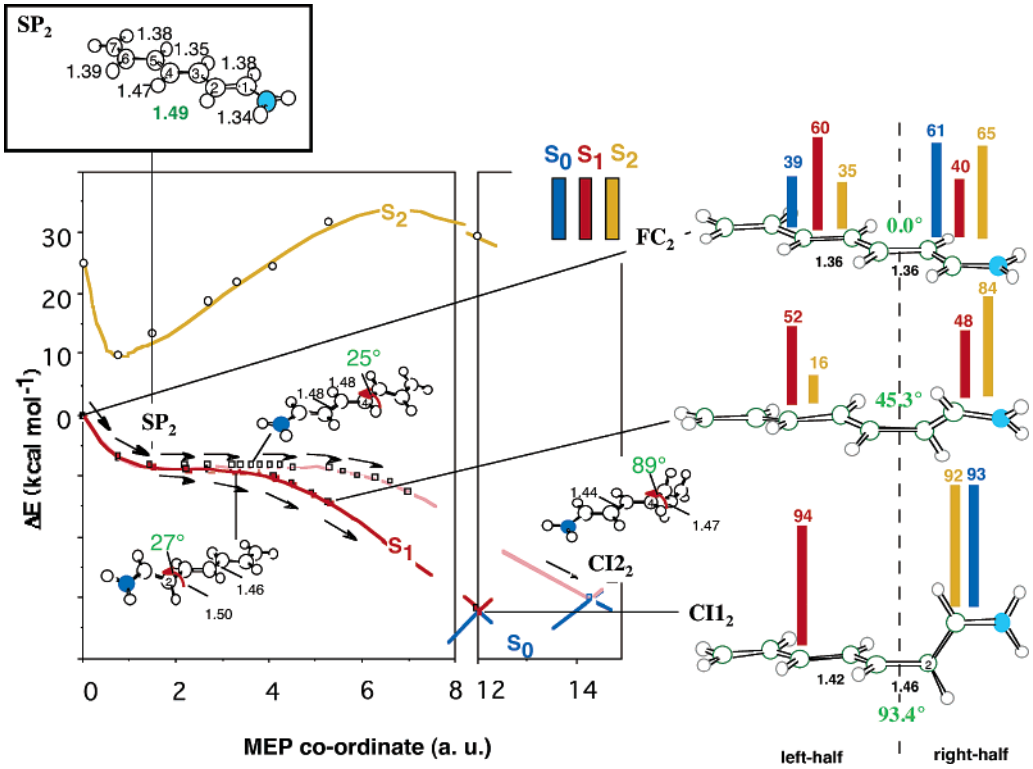


***Figure 3.*** Computed MEPs (see refs 8 and 10) for the competitive excited-state isomerizations of model **2** (the paths have been scaled to match PT2 energy values). Bar diagrams give the $S_0$, $S_1$, and $S_2$ (CAS-SCF 6-31G* Mulliken) charges for the $H_2C{=}CH{-}CH{=}CH{-}CH$ (left diagrams) and $CH{-}CH{=}NH_2$ (right diagrams) moieties along the path leading to the degenerate $S_1{\rightarrow}S_0$ decay funnel **CI1₂**. The structures (geometrical parameters in Å and degrees) document the progression of the molecular structure along the coordinate. **FC₂** is the Franck−Condon structure, **SP₂** corresponds to the $S_1$ relaxed planar species, and **CI1₂** and **CI2₂** are the competitive ∼90° twisted $S_1/S_0$ conical intersection decay funnels.

In conclusion, we have provided computational evidence suggesting a counterion-position dependent reaction stereoselectivity. As we will discuss later these results seem to provide a basis for understanding the photoisomerization selectivity in the protein environment.

**4.2. C-Tail Position.** The internal double-bond $S_1$ isomerization paths computed for model **2c** are collected in Figure 6. In contrast to models **2a** and **2b** one finds the following:

(i) the $S_1{-}S_0$ energy gap drops to ca. 65 kcal/mol;

(ii) a planar minimum (**SP$_{2c}$**) with a mixed covalent/charge-transfer electronic character (see the bar diagrams for the charges in Figure 6a) exists on $S_1$;

(iii) the $S_1$ isomerization paths are flat and display slight energy barriers (i.e., very low energy TSs). Furthermore, $S_1$ smoothly changes into a fully covalent electronic state along the paths to the twisted region (see the bar diagrams in Figure 6);

(iv) only the twisting of the terminal carbon−carbon double bond involves a real crossing point (**CI$_{2c}$**, Figure 6a), while covalent twisted minima (**TM1$_{2c}$** and **TM2$_{2c}$**) are involved in the rotation of the internal carbon−carbon double bonds (Figure 6b and c);

(v) an increasing $S_1{-}S_0$ energy gap separation is observed at the ending twisted structures (from 0 at the CI to ∼32 kcal/mol) as the rotating bond gets more and more distant from the countercharge.

The reasons of such a big modification in the photochemical properties and reactivity of **2c** as compared to the **Central** positions (**2a** and **2b**) or isolated system (**2**) can be easily understood recalling the qualitative schemes in section 3 (the same argument is true for **1b**, as reported in the Supporting Information). The counterion electrostatic effect downshifts (i.e., we have a red-shift) the ionic $S_1$ surface toward the covalent $S_0$ state (see Scheme 2), and this effect is even more pronounced proceeding along the isomerization coordinate (see Scheme 4b), leading to an anticipated crossing between $S_1$ and $S_0$. Due to that, an early mixing of the ionic and covalent states occurs that is already affective at the relaxed **SP$_{2c}$** point: in fact a mixed ionic−covalent structure is observed here with partial closed shell character. For these reasons the planar optimized structure **SP$_{2c}$** is structurally different from the one found in **2** (**SP$_2$**, see Figure 3), leading to substantially shorter C−C double bonds. Moreover, while in **2** this is a very shallow saddle point (i.e., $S_1$ displays antibonding character about central double-bond rotation), it is a real minimum in **2c**.[79] Therefore, energy barriers (although very small, less than 2 kcal/mol, as seen in Figure 6) are involved along the corresponding isomerization processes, while $S_1$ smoothly changes into a pure covalent (diradical) state on the way to the twisted region (see charge distribution bar diagrams in Figure 6).

As qualitatively predicted by Scheme 5b(ii), the CIs (see Figure 3) found in the isolated system **2** for the central C=C bond TICT points (**CI1₂** and **CI2₂**) are moved higher in energy by electrostatic interactions, and their topography may change from *peaked* to *sloped*. This leads to twisted covalent minima at the bottom of the $S_1$ surface (**TM1$_{2c}$** and **TM2$_{2c}$**), with significant $S_1{-}S_0$ energy separation. This energy gap decreases as the twisted bond approaches the countercharge (∼32, ∼17, and 0 kcal/mol respectively), finally leading to a *peaked* CI

(79) Ruiz, D. S.; Cembran, A.; Garavelli, M.; Olivucci, M.; Fuss, W. *Photochem. Photobiol.* **2002**, *76*, 622.

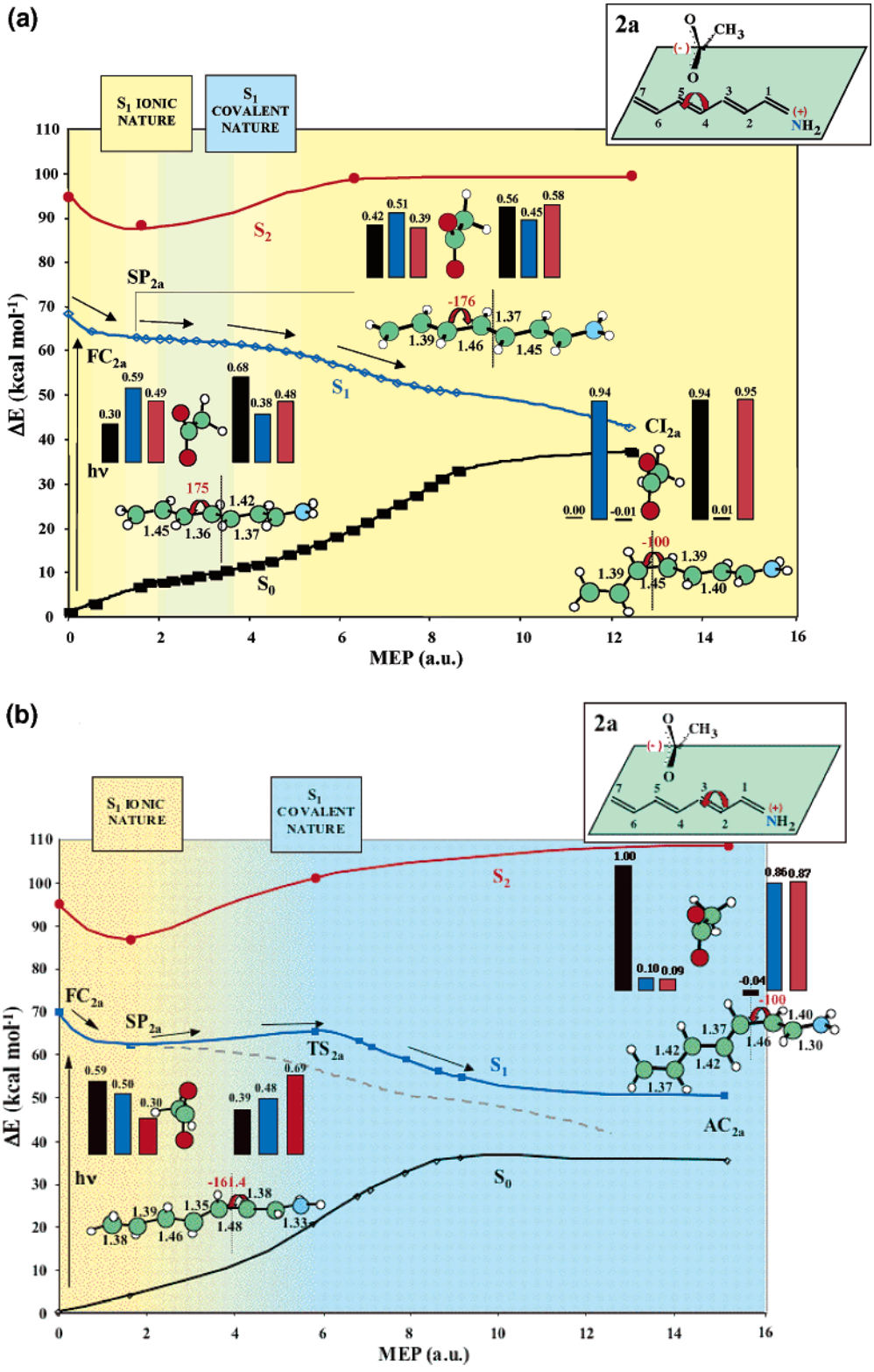


***Figure 4.*** Computed MEPs for **2a** along the (a) $S_1$ C4═C5 photoisomerization coordinate and (b) $S_1$ C2═C3 photoisomerization coordinate (the first path is also reported here for comparison: see the dotted gray line). Energy profiles have been scaled to match CASPT2 energies. The structures (geometrical parameters in Å and degrees) document the progression of the molecular structure along the coordinate. **$FC_{2a}$** is the Franck−Condon structure, **$SP_{2a}$** corresponds to the $S_1$ skeletal relaxed species, [78] **$CI_{2a}$** and **$TM_{2a}$** are the twisted $S_1/S_0$ conical intersection funnel and minimum, respectively, and **$TS_{2a}$** is the transition state located along the C2═C3 photoisomerization path. Ionic-like and covalent-like $S_1$ surfaces are illustrated by yellow and blue background colors, respectively. The bar diagrams give the $S_0$, $S_1$, and $S_2$ (CAS-SCF 6-31G* Mulliken) charges for the left and right moieties (see the dotted lines for the demarcation point) along the $S_1$ paths leading to the twisted region.

(**$CI_{2c}$**) for the isomerization of the terminal C═C bond, opening the way to a very efficient (almost barrierless) radiationless decay channel involving isomerization of the terminal methylene. This represents a path of no chemical significance, at least for the 7-unsubstituted systems. The trend observed in the $S_1$−$S_0$ energy gap at the twisted points can be easily explained since

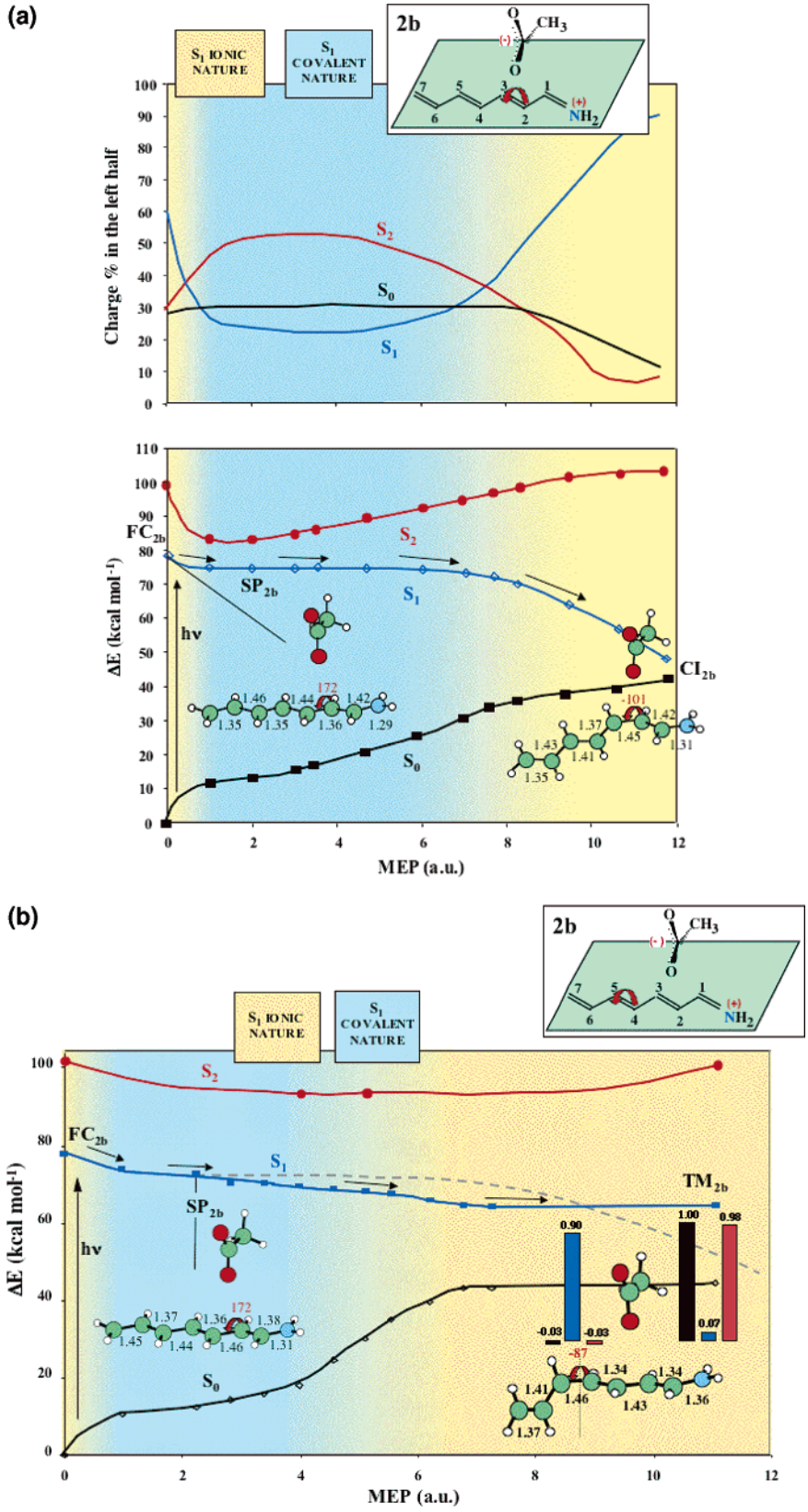


***Figure 5.*** Computed MEPs for **2b** along the (a) $S_1$ C2═C3 photoisomerization coordinate (bottom)[100] and (b) $S_1$ C4═C5 photoisomerization coordinate (the first path is also reported here for comparison: see the dotted gray line). Energy profiles have been scaled to match CASPT2 energies. The structures (geometrical parameters in Å and degrees) document the progression of the molecular structure along the coordinate. $\mathbf{FC_{2b}}$ is the Franck−Condon structure, $\mathbf{SP_{2b}}$ corresponds to the $S_1$ skeletal relaxed species,[78] and $\mathbf{CI_{2b}}$ and $\mathbf{TM_{2b}}$ are the TICT $S_1/S_0$ conical intersection funnel and minimum, respectively. Ionic-like and covalent-like $S_1$ surfaces are illustrated by yellow and blue background colors, respectively. Figure 5a (top) displays the progression of the positive (CAS-SCF 6-31G* Mulliken) charge located on the left isomerizing moiety along the $S_1$ path (bottom), while the bar diagrams in Figure 5b give the $S_0$, $S_1$, and $S_2$ (CAS-SCF 6-31G* Mulliken) charges for the left and right moieties (dotted line is the demarcation point) along the illustrated photoisomerization path.

*Scheme 6*

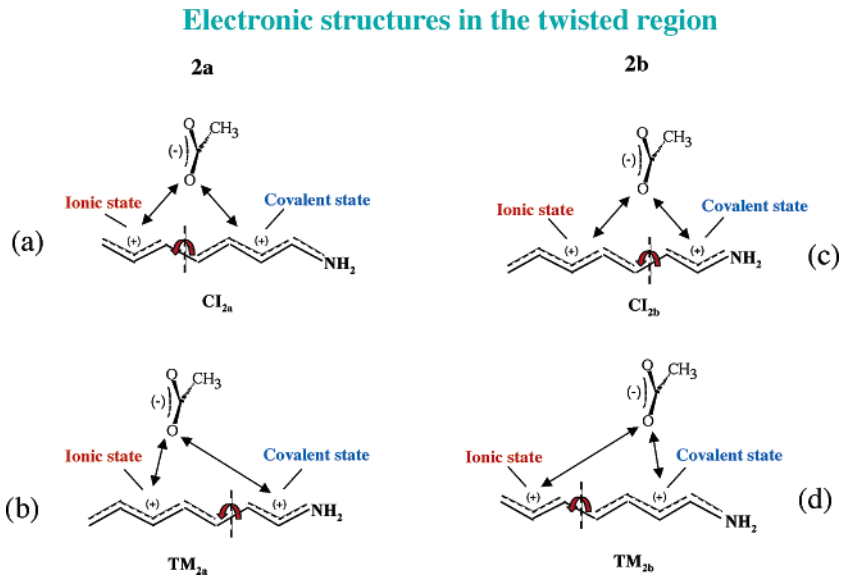


the positive/negative charge separation decreases as the rotating bond approaches the anion (see also Scheme 5b and discussion in section 3).

**4.3. N-Head Position.** Photoisomerization paths computed for model **2d** are reported in Figures 7 and 8. All the qualitative features presented in point (c) of section 3.1 and illustrated in Scheme 3 can be foreseen quantitatively here (as also in model **1c**, see the Supporting Information), namely:

(i) a marked blue-shift in the absorption that increases to ∼90 kcal/mol;

(ii) a well-defined diradical-type covalent minimum (**SP$_{2d}$**) on $S_1$ which is populated via relaxation from the FC region;

(iii) covalent/ionic avoided crossing TSs (leading to significant energy barriers along all the photoisomerization paths investigated here; see Figure 7), which restore the ionic charge transfer (i.e., hole-pair) character of the $S_1$ surface and drive the system into a TICT state on $S_1$;

(iv) a TICT real crossing point (i.e., a *peaked* CI) for the terminal C═N double-bond rotation (**CI1$_{2d}$**), while twisted minima for all the other $S_1$ optimized TICT structures involve rotation of internal C═C double bonds (**TM1$_{2d}$** and **TM2$_{2d}$**);

(v) an increasing $S_1-S_0$ energy gap at the TICT structures (from 0 − at the CI − to ∼30 kcal/mol) as the rotating bond gets more and more distant from the countercharge;

(vi) covalent low energy polyene-like isomerization paths driving the system to −(CH)$_3$− kinked conical intersection funnels (**CI2$_{2d}$** and **CI3$_{2d}$**), as the ones occurring in octatetraene and nonpolar polyenes in general (see Figure 8).[60,61,73,76,80]

The qualitative picture reported in Scheme 3 can be used to rationalize these results. Stabilization of the covalent and destabilization of the ionic states in the *head* position is very strong and makes the $S_1$ (ionic) and $S_2$ (covalent) states very close in energy already at the FC point. They do cross each other (i.e., we have an avoided crossing) early along the relaxation path from FC (due to the higher steepness of the covalent than the ionic state).[61,70] Therefore, $S_1$ changes into a covalent-type state, which drives the system into a relaxed planar diradical-type minimum (**SP$_{2d}$**) as it happens in neutral polyenes.[60,61,73,76,80] Here, $S_1$ is fully covalent, and single bond flip isomerization paths all involve CAS−SCF energy barriers via a second (covalent/ionic) avoided-crossing TS, which in fact restores the ionic charge-transfer nature of $S_1$ and funnels the system into a TICT point. PT2 corrections move these transition structures closer to the **SP$_{2d}$** point and at lower energies (see Table 2 and Figure 7); still they do not disappear, resulting in barrier controlled paths, which drive the system into ionic twisted minima (**TM1$_{2d}$** and **TM2$_{2d}$**) for internal bond rotations and a real crossing TICT point (**CI1$_{2d}$**) for C═N isomerization. $S_1-S_0$ energy gaps at the TICT points (∼30, ∼12, and 0 kcal/mol, respectively) are more or less the same as those computed for the *tail* and show the same trend. This is not surprising, since the distances between the twisted double bonds and the countercharge are similar in the two cases: as more distant is the countercharge from the rotating bond and as the positive/negative charge distance is longer, the larger the $S_1-S_0$ energy separation at the twisted point (see Scheme 5c).

As expected (see Scheme 5c), the TICT state for the terminal C═N bond twisting corresponds to a real crossing point (i.e., a *peaked* CI), since it is the one closer to the anion. Anyway, this channel is not the only one responsible for a thermally activated (i.e., barrier controlled) efficient radiationless deactivation of the system. Due to the countercharge stabilization of the covalent state, whole regions of the $S_1$ surface preserve their covalent (dot−dot) electronic character, and other competitive (i.e., low energy barrier) fully covalent paths on $S_1$ exist leading to conical intersection points (**CI2$_{2d}$** and **CI3$_{2d}$**; see Table 2 and Figure 8). These paths very much resemble the radiationless decay channels found in octatetraene and photoexcited neutral polyenes in general, leading to triradicaloid −(CH)$_3$− kinked conical intersection structures.[13,61,64,73,74] Therefore, covalent photochemistry and polyene-type photoproducts become accessible to photoexcited PSBs in **2d**-like geometric arrangements: this represents a striking difference with respect to the ionic-$S_1$ driven photochemistry found in isolated PSBs (**1**, **2**, **3**, and **4**).

## 5. Two-State or Three-State Model?

According to CASPT2//CASSCF results, photoisomerization paths for isolated PSBs (**1**, **2**, **3**, and **4**) have been described via a *two-state/two-mode* reactivity model,[10] as seen in section 1. This model significantly differs from the alternative three-state

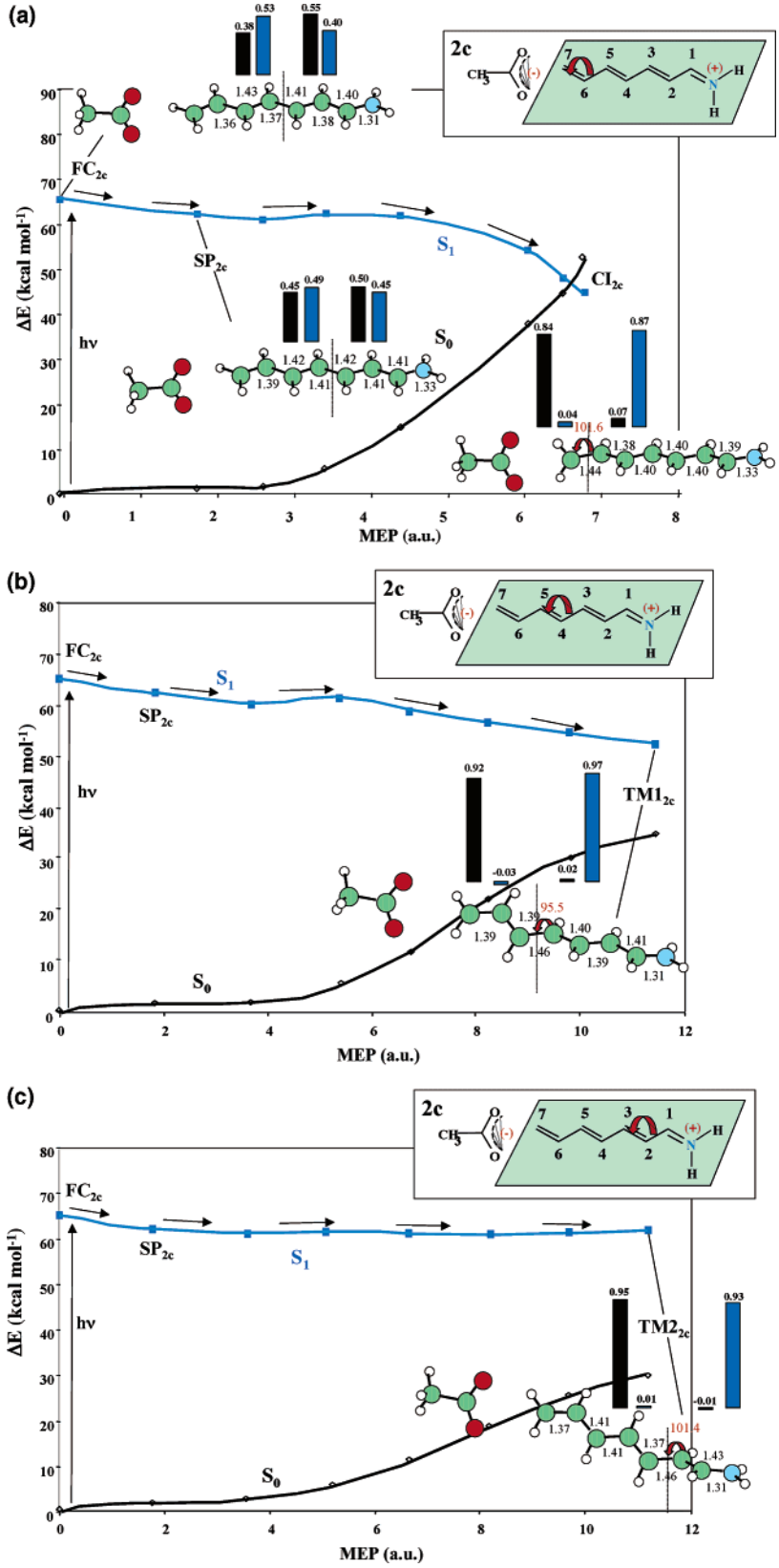


***Figure 6.*** Computed MEPs[100] for **2c** along the (a) $S_1$ C6═C7 photoisomerization coordinate, (b) $S_1$ C4═C5 photoisomerization coordinate, and (c) $S_1$ C2═C3 photoisomerization coordinate. Energy profiles have been scaled to match CASPT2 energies. The structures (geometrical parameters in Å and degrees) document the progression of the molecular structure along the coordinate. **$FC_{2c}$** is the Franck−Condon structure; **$SP_{2c}$** corresponds to the $S_1$ skeletal relaxed species; and **$CI_{2c}$**, **$TM1_{2c}$**, and **$TM2_{2c}$** are the twisted $S_1/S_0$ conical intersection funnel and minima, respectively. The bar diagrams give the $S_0$ and $S_1$ (CAS-SCF 6-31G* Mulliken) charges for the left and right moieties (see the dotted lines for the demarcation point) of **2c** along the illustrated photoisomerization paths.

model also used for retinals[81] (coming from nonpolar polyenes photochemistry), where a covalent diradical-type $S_1$ state drives the dynamics and accounts for the photochemical behavior of the excited system. Remarkably, compelling results in this field

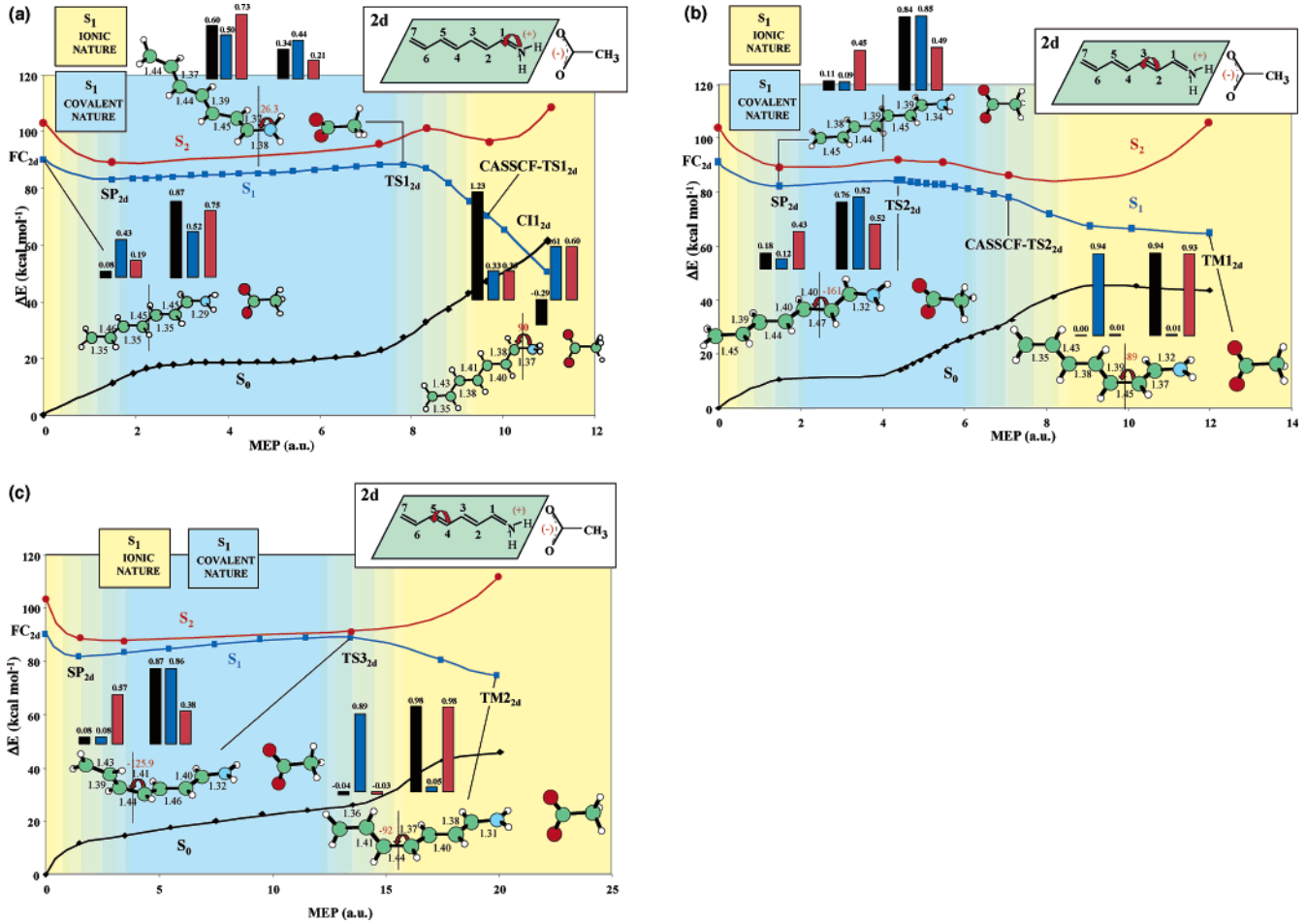


***Figure 7.*** Computed MEPs for **2d** along the (a) $S_1$ N═C1 photoisomerization coordinate, (b) $S_1$ C2═C3 photoisomerization coordinate, and (c) $S_1$ C4═C5 photoisomerization coordinate. Energy profiles have been scaled to match CASPT2 energies. The structures (geometrical parameters in Å and degrees) document the progression of the molecular structure along the coordinate. $\mathbf{FC_{2d}}$ is the Franck−Condon structure; $\mathbf{SP_{2d}}$ corresponds to the covalent-$S_1$ skeletal relaxed species; $\mathbf{CI1_{2d}}$, $\mathbf{TM1_{2d}}$, and $\mathbf{TM2_{2d}}$ are the TICT $S_1/S_0$ conical intersection funnel and minima, respectively; and $\mathbf{TS1_{2d}}$, $\mathbf{TS2_{2d}}$, and $\mathbf{TS3_{2d}}$ are the transition states located along the paths. Ionic-like and covalent-like $S_1$ surfaces are illustrated by yellow and blue background colors, respectively. The bar diagrams give the $S_0$, $S_1$, and $S_2$ (CAS-SCF 6-31G* Mulliken) charges for the twisting left and right moieties (dotted lines represent the demarcation point) of **2d** along the illustrated photoisomerization paths.

have shown that a covalent/covalent real crossing strongly differs (both in the geometric and electronic structure) by an ionic/covalent conical intersection, the former being an asymmetric highly uncoupled polyradicaloid systems,[61,64,73,74,82] with the latter being a TICT state.[7,9,10,13,49,75,79] While the first funnels a radiationless decay that hardly leads to high photoisomerization QYs,[60,73,76,80] the second drives efficient double-bond isomerizations, as the ones observed (both in vivo and in solution) for PSBs.

Anyway, the computational results presented here show that, according to some specific cation/anion arrangements, a crossing between $S_1$ and $S_2$ can occur, and the relaxed $S_1$ state (SP) can become a covalent (dot-dot) diradical type. For example, in the **N-head** position (**1c**, **2d**) the covalent excited state becomes more stabilized and eventually crosses the ionic state, leading to a lower energy covalent $S_1$ surface, as it happens in nonpolar conjugated hydrocarbons. Therefore, it might be questionable if the simple two-state reactivity model presented above for isolated PSBs retains its validity and is still of general applicability. Nevertheless, as we will shortly show, a deeper analysis of the electronic nature of all the computed one-bond flip photoisomerization channels support this view and call for the two-state model as being a *generally valid reactivity scheme* for PSB cis−trans photoisomerizations.

A convincing proof can be simply provided by the analysis of the geometrical and electronic structure that the system displays at the end of all the computed excited-state one-bond flip paths (i.e., the optimized twisted structures at the bottom of the $S_1$ surface): *in all cases* this has the form of a twisted minimum (TM) or real crossing (i.e., a *peaked* CI) between the ionic and the covalent $S_1$ and $S_0$ states (whatever the specific energy order of the two surfaces!). Here, the covalent (diradical type) singlet excited-state $S_2$ is far higher in energy and does not become involved in the process. This evidence should already be convinccing that the two-state model for the one-bond flip mechanism works properly whatever the geometric arrangement with the countercharge. Still, a more systematic description is perhaps preferred. For this purpose we will classify the paths according to the number of avoided crossings encountered along the channel before reaching the twisted region:

(a) **Two avoided crossings**: All one-bond flip MEPs computed for **2b** and **2d** (and for **1c**; see the Supporting

(80) Garavelli, M.; Celani, P.; Yamamoto, N.; Bernardi, F.; Robb, M. A.; Olivucci, M. *J. Am. Chem. Soc.* **1996**, *118*, 11656.
(81) Hasson, K. C.; Gai, F.; Anfinrud, P. A. *Proc. Natl. Acad. Sci. U.S.A.* **1996**, *93*, 15124.

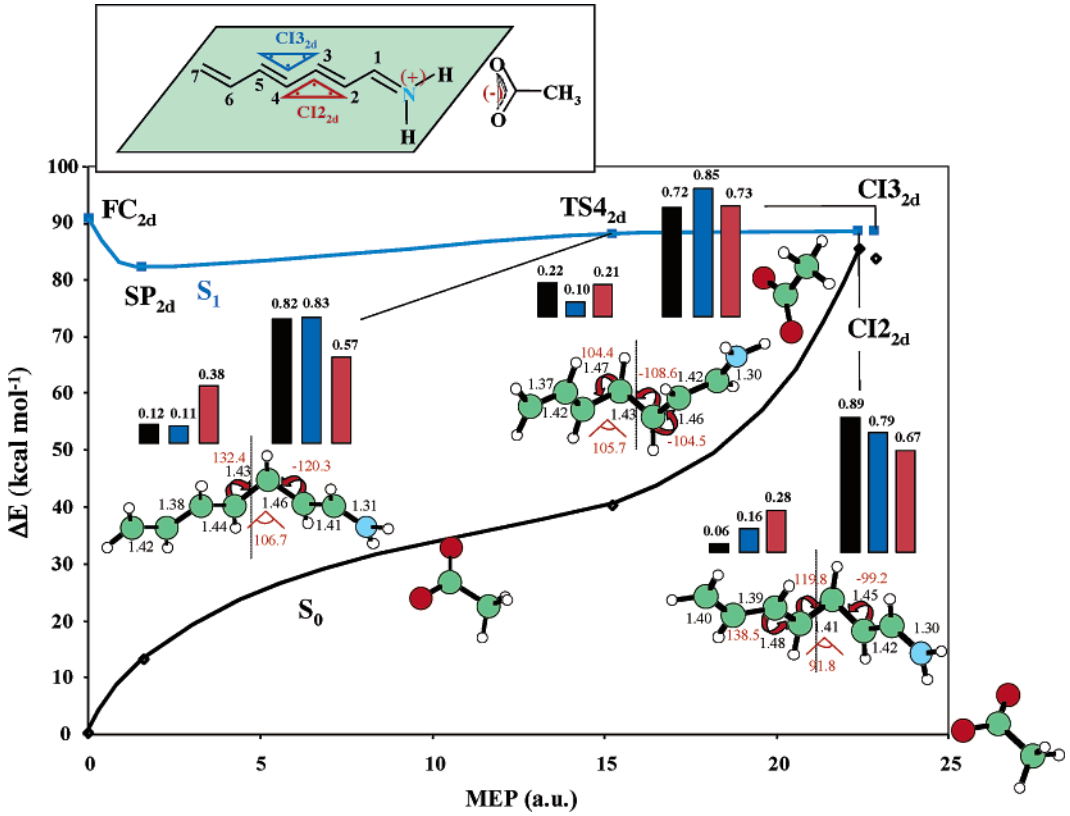


***Figure 8.*** Computed MEP along a competitive fully covalent $S_1$ radiationless decay channel leading to a low energy $S_1/S_0$ conical intersection of the kink type, involving the C2−C3−C4 triangular fragment (**CI2$_{2d}$**) of **2d**. Another conical intersection (**CI3$_{2d}$**), involving the C3−C4−C5 triangular fragment, has been reported here but no MEP has been calculated. The two triradicaloid kinks involved in **CI2$_{2d}$** and **CI3$_{2d}$** have been highlighted on the structure reported in the top left box. Energy profiles have been scaled to match CASPT2 energies. The structures (geometrical parameters in Å and degrees) document the progression of the molecular structure along the coordinate. **FC$_{2d}$** is the Franck−Condon structure, **SP$_{2d}$** corresponds to the covalent-$S_1$ skeletal relaxed species, and **TS4$_2$** is the transition state leading to **CI2$_{2d}$**.

Information) involve two consecutive $S_1/S_2$ avoided crossings, the first changing the nature of the $S_1$ surface from ionic (FC) to covalent (SP), the second restoring its ionic charge-transfer character (and often leading to an avoided crossings TS). The covalent excited singlet state (double HOMO→LUMO excitation type) becomes involved only at the very initial stage of the relaxation process, but after the second crossing it goes higher in energy (due to its bonding character) and never becomes involved again. Eventully, it is still the ionic $S_1$ state that drives the system into the TICT points, as for the isolated systems. Therefore, at the very initial stage of the dynamics out of the FC region, PSBs photoisomerization is still driven according to a two-state model.

(b) **One avoided crossing**: The $C_2$═$C_3$ isomerization MEP in **2a** and all one-bond flip MEPs computed for **2c** (and for **1b**; see the Supporting Information) involve a single ionic/covalent avoided crossing between $S_1$ and $S_0$. For these paths the validity of the two-state model is even more evident: in fact, the covalent HOMO→LUMO double-excitation type $S_2$ state is too high in energy all along the path to affect the mechanism, even higher (due to the countercharge effects) than in the isolated models. The single $S_1/S_0$ avoided crossing has only the effect to swap the order between ionic and covalent surfaces for $S_1$ and $S_0$: the $S_1$ surface changes from ionic (FC) to covalent (via a mixed ionic/covalent SP structure for **1b** and **2c**), while $S_0$ becomes a ionic charge transfer state. Although it is now a covalent $S_1$ state that drives the system into the twisted minimum, this is diabatically connected to the covalent $S_0$ state in the FC (while $S_0$ is diabatically connected to the ionic $S_1$ state in the FC). Again, the reactivity can be depicted using a two-state model, although the order of the two states becomes inverted as the twisted point is approached.

(c) **No avoided crossings**: These results (i.e., the one-bond flip path computed for **1a** (see the Supporting Information) and $C_4$═$C_5$ isomerization in **2a**) are substantially identical to those computed for the isolated models (**1** and **2**). The excited $S_1$ state preserves its ionic charge transfer character all along the path until it is to the TICT CI with the covalent ground-state $S_0$. Since no qualitative differences exist with the isolated systems, the previously proposed two-state model perfectly fits.

It is worth noting that, besides the two-state one-bond flip reactivity model, also a competitive covalent photochemistry can become accessible for **1c** and **2d** due to the strong stabilization of the excited covalent state (see Figure 8 and Figure S4 in the Supporting Information). Still, these covalent channels are totally different than the ionic one-bond flip ones (and are slightly higher in energy, i.e., less favored). While the former lead to kinked conical intersections as found in polyenes (and cannot lead to high QYs for C−C double-bond isomerization), the latter are still the only ones describing efficient E→Z isomerizations (the excited state deactivation funnel being a double-bond fully twisted structure, which easily drives a double-bond rotation, unlike the kinked CIs). Therefore, a branching in the $S_1$ photochemistry can become possible for **1c** and **2d**: a covalent one (following a three-state reactivity model as in nonpolar polyenes, still less favored) and an ionic one

***Table 2.*** CASSCF/6-31g* Absolute and CASPT2/6-31G* Absolute and Relative State Average Energies (a Three-Root CASSCF for **2a** and **2b**, a Two-Root CASSCF for 2**c**, and a Four-Root CASSCF for **2d** (Only the First Three Roots Are Reported in This Case) Have Been Used with Equal Weights for the States); the Weight ($\omega$) of the Zeroth Order CASSCF Wave Function in the CASPT2 Wave Function is also Reported

| structure[a] | state | CASSCF [a] (au) | CASPT2 (au) | $\omega$ | $\Delta E$ eV (kcal mol$^{-1}$) | structure[a] | state | CASSCF [a] (au) | CASPT2 (au) | $\omega$ | $\Delta E$ eV (kcal mol$^{-1}$) |
|---|---|---|---|---|---|---|---|---|---|---|---|
| | | | Model **2a** | | | | | | Model **2d** | | |
| $FC_{2a}$ | $S_0$ | −552.492 27 | −554.068 34 | 0.66 | 0.00 (0.0) | $FC_{2d}$ | $S_0$ | −552.557 83 | −554.117 34 | 0.67 | 0.00 (0.0) |
| | $S_1$ | −552.359 83 | −553.957 15 | 0.64 | 3.03 (69.8) | | $S_1$ | −552.343 60 | −553.972 41 | 0.63 | 3.94 (90.9) |
| | $S_2$ | −552.319 50 | −553.916 92 | 0.61 | 4.12 (95.0) | | $S_2$ | −552.374 17 | −553.953 84 | 0.66 | 4.45 (102.6) |
| $SP_{2a}$[78] | $S_0$ | −552.480 25 | −554.061 69 | 0.66 | 0.18 (4.2) | $SP_{2d}$ | $S_0$ | −552.530 23 | −554.098 07[b] | 0.1[b] | 0.52 (12.1)[b] |
| | $S_1$ | −552.369 28 | −553.966 92 | 0.61 | 2.76 (63.6) | | | | [−554.097 26][b] | [0.66][b] | [0.54 (12.4)][b] |
| | $S_2$ | −552.330 07 | −553.928 44 | 0.59 | 3.81 (87.8) | | $S_1$ | −552.413 31 | −553.985 42 | 0.66 | 3.59 (82.8) |
| $CI_{2a}$ | $S_0$ | −552.420 68 | −554.008 90 | 0.66 | 1.62 (37.3) | | | | [−553.985 05] | [0.66] | [3.59 (82.8)][b] |
| | $S_1$ | −552.396 08 | −553.999 51 | 0.60 | 1.87 (43.2) | | $S_2$ | −552.350 84 | −553.974 80 | 0.55 | 3.88 (89.4) |
| | $S_2$ | −552.310 19 | −553.909 55 | 0.48 | 4.32 (99.6) | SP-$ion_{2d}$ | $S_0$ | −552.544 35 | −554.108 98 | 0.67 | 0.23 (5.2) |
| $TS_{2a}$ | $S_0$ | −552.450 55 | −554.034 93 | 0.66 | 0.91 (21.0) | | $S_1$ | −552.361 45 | −553.988 72 | 0.64 | 3.50 (80.7) |
| | $S_1$ | −552.369 24 | −553.964 15 | 0.65 | 2.84 (65.4) | | $S_2$ | −552.403 39 | −553.975 49 | 0.66 | 3.86 (89.0) |
| | $S_2$ | −552.310 06 | −553.904 48 | 0.63 | 4.45 (102.8) | $TS1_{2d}$ | $S_0$ | −552.508 58 | −554.082 16 | 0.66 | 0.96 (22.1) |
| $TM_{2a}$ | $S_0$ | −552.406 92 | −554.012 17 | 0.65 | 1.53 (35.2) | | $S_1$ | −552.400 60 | −553.977 69 | 0.58 | 3.80 (87.6) |
| | $S_1$ | −552.414 76 | −553.988 68 | 0.66 | 2.17 (50.0) | | $S_2$ | −552.338 62 | −553.964 74 | 0.63 | 4.15 (95.8) |
| | $S_2$ | −552.315 97 | −553.893 97 | 0.64 | 4.74 (109.4) | $CI1_{2d}$ | $S_0$ | −552.399 52 | −554.038 22 | 0.64 | 2.16 (49.7)[c] |
| | | | Model **2b** | | | | $S_1$ | −552.450 43 | −554.018 42 | 0.65 | 2.69 (62.1)[c] |
| $FC_{2b}$ | $S_0$ | −552.510 94 | −554.080 05 | 0.67 | 0.00 (0.0) | | $S_2$ | −552.368 91 | −553.945 26 | 0.49 | 4.68 (108.0) |
| | $S_1$ | −552.348 26 | −553.955 37 | 0.64 | 3.39 (78.2) | $TS2_{2d}$ | $S_0$ | −552.525 61 | −554.091 72 | 0.63 | 0.70 (16.1) |
| | $S_2$ | −552.329 22 | −553.920 01 | 0.60 | 4.35 (100.4) | | $S_1$ | −552.410 79 | −553.982 61 | 0.64 | 3.66 (84.5) |
| $SP_{2b}$[78] | $S_0$ | −552.486 76 | −554.062 00 | 0.66 | 0.49 (11.3) | | $S_2$ | −552.347 42 | −553.967 67 | 0.64 | 4.07 (93.9) |
| | $S_1$ | −552.369 29 | −553.959 72 | 0.64 | 3.27 (75.5) | $TM1_{2d}$ | $S_0$ | −552.475 40 | −554.041 12 | 0.66 | 2.07 (47.8) |
| | $S_2$ | −552.342 82 | −553.947 59 | 0.60 | 3.60 (83.1) | | $S_1$ | −552.399 71 | −554.022 82 | 0.65 | 2.57 (59.3) |
| $CI_{2b}$ | $S_0$ | −552.437 40 | −554.012 83 | 0.66 | 1.83 (42.2) | | $S_2$ | −552.374 29 | −553.949 25 | 0.57 | 4.58 (105.5) |
| | | | [−554.011 35][b] | [0.66][b] | [1.83 (42.2)][b] | $TS3_{2d}$ | $S_0$ | −552.506 72 | −554.075 07 | 0.66 | 1.15 (26.5) |
| | $S_1$ | −552.397 82 | −554.000 31[b] | 0.02[b] | 2.17 (50.0)[b] | | $S_1$ | −552.398 00 | −553.974 89 | 0.63 | 3.88 (89.4) |
| | | | [−554.002 95][b] | [0.65][b] | [2.06 (47.5)][b] | | $S_2$ | −552.337 25 | −553.971 50 | 0.64 | 3.97 (91.5) |
| | $S_2$ | −552.335 05 | −553.914 01 | 0.43 | 4.52 (104.2) | $TM2_{2d}$ | $S_0$ | −552.478 75 | −554.045 22 | 0.66 | 1.96 (45.3) |
| $TM_{2b}$ | $S_0$ | −552.420 03 | −554.007 47 | 0.66 | 1.97 (45.5) | | | | [−554.044 37][b] | [0.66][b] | [1.96 (45.3)][b] |
| | $S_1$ | −552.374 92 | −553.980 57 | 0.65 | 2.71 (62.4) | | $S_1$ | −552.375 71 | −553.998 45 | 0.65 | 3.24 (74.6) |
| | $S_2$ | −552.323 49 | −553.920 29 | 0.59 | 4.35 (100.2) | | $S_2$ | −552.368 87 | −553.938 50[b] | 0.36[b] | 4.87 (112.2)[b] |
| | | | Model **2c** | | | | | | [−553.944 17][b] | [0.66][b] | [4.69 (108.2)][b] |
| $FC_{2c}$ | $S_0$ | −552.488 97 | −554.067 52 | 0.66 | 0.00 (0.0) | $TS4_{2d}$ | $S_0$ | −552.483 41 | −554.053 09 | 0.66 | 1.75 (40.3) |
| | $S_1$ | −552.372 51 | −553.963 63 | 0.65 | 2.83 (65.2) | | $S_1$ | −552.397 25 | −553.977 37 | 0.64 | 3.81 (87.8) |
| $SP_{2c}$ | $S_0$ | −552.485 46 | −554.065 34 | 0.66 | 0.06 (1.4) | | $S_2$ | −552.325 37 | −553.935 95 | 0.59 | 4.93 (113.8) |
| | $S_1$ | −552.377 31 | −553.968 02 | 0.65 | 2.71 (62.4) | $CI2_{2d}$ | $S_0$ | −552.400 26 | −553.980 42 | 0.66 | 3.73 (85.9) |
| $CI_{2c}$ | $S_0$ | −552.385 90 | −553.992 92 | 0.65 | 2.03 (46.8) | | $S_1$ | −552.394 83 | −553.976 45 | 0.65 | 3.83 (88.4) |
| | $S_1$ | −552.400 75 | −553.984 05 | 0.66 | 2.27 (52.4) | | $S_2$ | −552.289 61 | −553.875 08 | 0.52 | 6.59 (152.0) |
| $TM1_{2c}$ | $S_0$ | −552.424 97 | −554.010 92 | 0.66 | 1.54 (35.5) | $CI3_{2d}$ | $S_0$ | −552.381 77 | −553.983 99 | 0.64 | 3.63 (83.7) |
| | $S_1$ | −552.386 73 | −553.983 72 | 0.65 | 2.28 (52.6) | | $S_1$ | −552.388 11 | −553.976 45 | 0.65 | 3.83 (88.4) |
| $TM2_{2c}$ | $S_0$ | −552.430 93 | −554.019 70 | 0.66 | 1.30 (30.0) | | $S_2$ | −552.299 89 | −553.930 44 | 0.59 | 5.09 (117.3) |
| | $S_1$ | −552.374 67 | −553.968 44 | 0.65 | 2.70 (62.2) | $TS5_{2d}$[d] | $S_0$ | −552.528 69 | −554.095 71 | 0.65 | 0.59 (13.6) |
| | | | | | | | $S_1$ | −552.359 88 | −553.984 66 | 0.58 | 3.61 (83.3) |
| | | | | | | | $S_2$ | −552.400 12 | −553.975 47 | 0.55 | 3.86 (89.0) |

[a] All the FC and SP geometries are obtained with single-root CASSCF optimizations (CASSCF energies not given), while two-root or three-root state average CASSCF calculations (equal weights for the states) have been used for all the other structures reported. [b] In a few cases (reported in italic) the reference weight is smaller than 0.5. At these points a second set of calculations was then performed using increasing imaginary shift values (IMAG) (see: Forsberg, N.; Malmqvist, P. A.; *Chem. Phys. Lett.* **1997**, *274*, 196) in the CASPT2 calculation until the energy difference between $S_0$ (also shifted and reported in square brackets as reference) and the low-weight state becomes constant. In all the cases, an IMAG value of 0.05 was found to be enough to make the result stable. [c] It could seem, judging by the large energy difference between $S_0$ and $S_1$, that this point is not a conical intersection. Actually, conical intersection optimization involves a state average wave function between $S_0$ and $S_1$ (with equal weights), and a true degeneration point exists:

| Structure | State | CASSCF (au) | CASPT2 (au) | ω | ΔE kcal mol$^{-1}$ |
|---|---|---|---|---|---|
| $CI1_{2d}$ | $S_0$ | -552.43378 | -554.02944 | 0.65 | 0.0 |
| | $S_1$ | -552.43166 | -554.02783 | 0.65 | 1.0 |

The results reported in the Table are obtained, instead, by equally weighting the first four singlet roots, which slightly shifts the degeneracy at the CASSCF level. After CASPT2 corrections, wave function analysis shows that $S_0$ and $S_1$ have already swapped. This means that the conical intersection point comes earlier along the reaction coordinate by using a four-state state average procedure. [d] See Supporting Information.

(leading to barrierless or at least lower energy cis−trans photoisomerizations). This counterion dependent tuning in PSB photochemistry typology represents a new aspect of potential technological relevance that might be exploited in the design of PSB-based artificial chromophores.

Finally, it must be said that in all cases the photoisomerization reaction coordinate is similar to the one computed for isolated PSBs; i.e., the *two-mode* model for PSBs photoinduced molecular motion previously suggested[10] still retains its validity, although the specific planar stretching involving the initial relaxation out of the FC region can be different according to the ionic (**Central**), covalent (**N-head**), or mixed (**C-tail**) nature of the relaxed SP intermediate on $S_1$ populated by decay from the FC region.

## 6. A Unified View for Countercharge Intermolecular Effects

In this section we present a unified view for the computational results reported above. We will try to collect all the data into a single counterion-position dependent reactivity scheme that shows the effect of an external electrostatic field on the efficiency, rate, and selectivity of PSB photoisomerizations. Results from isolated systems will be also referred to and used

*Scheme 7*

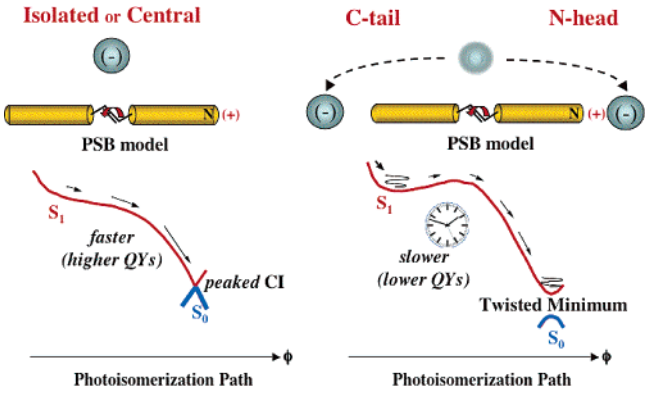


for comparative purposes. Speculations on the effects of countercharges in vivo and in solution will complement this view.

**6.1. Reaction Rate and Efficiency Control.** All the data collected for models **1**, **1a**, **1b**, **1c** and **2**, **2a**, **2b**, **2c**, **2d** show that the potential energy surface (PES) steepness along the computed photoisomerization MEPs and the $S_1-S_0$ energy gap in the twisted region can be tuned and controlled by the counterion position along the chain. Isolated systems (**1** and **2**) or **Central** models (**1a**, **2a**, and **2b**) display the most favored conditions for ultrafast and efficient central double-bond photoisomerizations, namely: (i) steep and/or barrierless isomerization paths and (ii) TICT conical intersection points of the *peaked* type for internal C−C double-bond flip, funneling an ultrafast and efficient radiationless decay that prompts a high photoisomerization QY. In fact, no thermal equilibration is expected, neither at the relaxed SP point on $S_1$ nor at the degenerate TICT structures. On the other hand, as the countercharge is moved backward to the **C-tail** (**1b**, **2c**) or forward to the **N-head** (**1c**, **2d**) of the system, a slower and less efficient photoisomerization process should be expected because (i) the $S_1$ PES steepness along the path decreases, (ii) a barrier can possibly emerge, and (iii) *peaked* conical intersections for internal C−C double-bond isomerizations are replaced by twisted minima (with significant energy gap separation between $S_1$ and $S_0$) at the bottom of the computed $S_1$ MEPs. Thermal equilibration at the relaxed SP minimum and/or at the twisted minima would delay the process, decreasing the radiationless decay rate, photoisomerization efficiency, and QYs (see Scheme 7). Efficient radiationless decay channels still exist but are thermally activated (i.e., there is a barrier) and only involve rotations about the terminal double bonds of the chain, i.e., are not of chemical significance.

In conclusion, our results show that the position of the external countercharge can be a suitable tool for tuning photoisomerization rate and efficiency: only when the countercharge is placed in a **Central** position or its effects are quenched (i.e., isolated systems), photoisomerization efficiency is magnified and very favored ultrafast (i.e. barrierless) radiationless decay channels are opened. On the other hand, electrostatic interaction with counterions at the **N-head** or the **C-tail** would result (although for different reasons, see section 4) in slower and less efficient photoisomerizations and radiationless decays.

**6.2. Covalent vs Ionic Photochemistry.** Interaction with the countercharge can be exploited also to tune the nature and stability of the relaxed photochemically relevant $S_1$ state and, accordingly, to control or select the photochemical behavior of the system. According to our results (section 4.3), counterion **N-head** stabilization on covalent states can be so big that the relaxed $S_1$ state becomes covalent, as it happens in neutral polyenes. Consequently, one-bond flip isomerizations are made less favored (e.g., energy barriers emerge and *peaked* conical intersections disappear in the twisted region), while a competitive covalent photochemistry becomes accessible (see section 4): these new low energy counterion-stabilized channels drive PSBs toward covalent/covalent $-(CH)_3-$ kinked $S_1/S_0$ conical intersections, opening to photoexcited PSBs the covalent photochemistry found in nonpolar conjugated hydrocarbons, with their related photoproducts.

*Scheme 8*

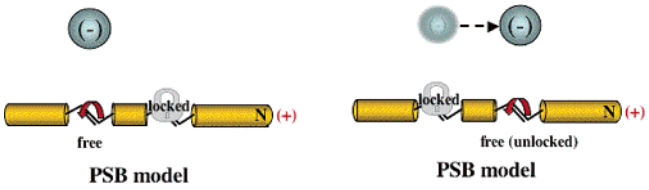


In conclusion, selection and control of the photochemical typology (i.e., ionic vs covalent) may be possibly achieved by counterion position.

**6.3. Photoisomerization Stereoselectivity Control.** Perhaps, one of the most remarkable results is that countercharge position does provide a valuable tool for selecting the double bond likely involved in the photoisomerization process. Moving the counterion above the molecular plane of the chromophore does effect competitive isomerizations for internal C−C double bonds (see **2a** and **2b**), opening or locking specific isomerization paths: a barrierless (i.e., efficient) photoisomerization leading to a TICT CI point (i.e., an ultrafast radiationless decay funnel) occurs only for the double bond being closer to the anion (i.e., the double bond right below it), while the other competitive path gets locked, or at least becomes much less favored (i.e., a barrier emerges along the path, and/or the *peaked* CI point disappears being replaced by a twisted minimum, which leads to thermal equilibrations); see Scheme 8.

An even more general result is that the *peaked* CIs found in the twisted region *follow* the counterion along the chain of the chromophore; i.e., they do involve the rotation of the double bond closer to the anion. This means that highly efficient radiationless decay channels (although these can be barrier controlled, i.e., thermally activated; see **1b**, **1c**, **2c**, and **2d**) should only exist for photoisomerizations occurring in the vicinity of the countercharge. Anyway, only for the **Central** positions (**1a**, **2a**, and **2b**) steep barrierless paths exist (or at least the energy barrier gets negligible), therefore opening channels for highly efficient and ultrafast photoisomerizations.

We think all these features and stereoselective effects may represent technologically relevant information that must be taken into account in the future design of efficient PSB-based E→Z photoswitchable devices embedded in modified protein cavities or artificial biomimetic environments. Here, in fact, a suitable choice of the position of the PSB countercharge may be used to tune both the photochemical reactivity and the efficiency of the chromophore.

**6.4. Photoisomerization in the Protein Environment: Correlation between Computations and Observations.** The

***Scheme 9***

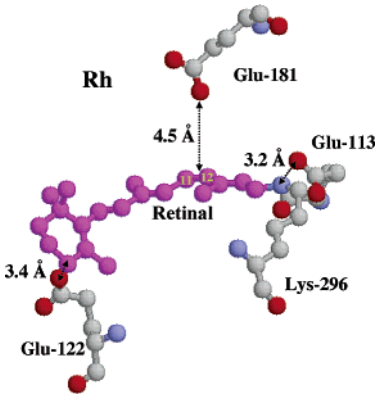


***Scheme 10***

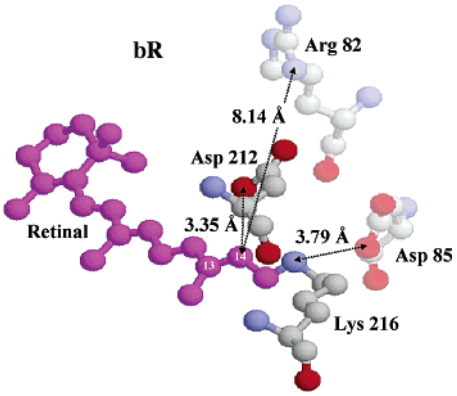


results of section 4 and the discussion of section 6.3 immediately suggest that the endogenous counterions of rhodopsin proteins can play a role in determining the observed photoisomerization stereoselectivity. In Scheme 9 we display the observed structure for the PSB11 chromophore in Rh,[52] together with the closer and most relevant polar groups surrounding it (i.e., the three glutamic acid residues Glu-113, Glu-181, and Glu-122). Interestingly, Glu-113, Glu-181, and Glu-122 are close to the **N-head**, **Central**, and **C-tail** positions of the chromophore, respectively. Except for the formal PSB counterion (i.e., Glu-113, which is likely to adopt an anionic form), the protonation state for the other two residues is not unambiguously known, although they are both assumed to be protonated. On one hand, Glu-122 has been reported to be neutral,[83] but site-specific mutagenesis of Glu-122 to Gln results in a significant blue-shift in the absorption maximum of the chromophore (from 500 to 480 nm) and a reduced transducing-stimulating activity.[84−86] This suggests that Glu-122 (if not fully deprotonated) at least supports a partial negative charge that contributes to the observed red-shift and assists isomerization by transient salt bridge formation with the **C-tail** cationic region of the excited chromophore (as we know, the positive charge migrates, upon excitation, from the **N-head** to the **C-tail**).[10,87] These findings might explain the high isomerization QY in the protein and why this residue, along with the Schiff base counterion Glu-113, is the most highly conserved membrane embedded carboxylate found in rhodopsins.[86,88,89] This **C-tail** polar residue may partially balance (i.e., quench) Glu-113 counterion effects at the **N-head**, thus leading to an isolated-like condition for the retinal chromophore.

Interestingly, Shakuray and co-worker[45] showed that the protein dielectric $\epsilon$ (even a value as small as $\epsilon = 4.0$, which is usually the assumed protein dielectric in the binding pocket) could also quench single countercharge effects. Remarkably, this working hypothesis has been recently validated by Ferre et al.[90] for the retinal chromophore in Rh by using highly correlated computations with a new hybrid QM(CAS//CASPT2)/MM(Amber) approach:[91] an overall isolated-like electrostatic environment around the chromophore has been found, although no charged residues but Glu-113 were considered.

Finally, no direct experimental information about the protonation state of Glu-181 is available up to date. Still, solid-state NMR spectroscopic measurements[41−43] predict a negative charge close to the isomerizing double bond (i.e., where Glu-181 is placed), and very recent molecular dynamics simulations on Rh[92] strongly suggest a deprotonated carboxylate for Glu-181. Therefore, whatever its real protonation state, it is very likely (according to the above data) that this group supports at least a partial negative charge. Very remarkably, this residue is right above the central $C_{11}$=$C_{12}$ isomerizing double bond of the chromophore,[52] in a geometric arrangement which very much resemble models **1a** and **2a**. Therefore, according to our results for the **Central** position (**1a**, **2a**), an electrostatically driven selection for the photoisomerization of the central $C_{11}$=$C_{12}$ bond should be expected. This effect might act in concert with the binding pocket steric interactions in catalyzing the photoisomerization of the central double bond and might represent the primary electrostatic factor responsible for photoisomerization catalysis.

A similar speculation can be extended also to the PSBT chromophore in bR (see Scheme 10). Very remarkably, here a negative carboxylate (i.e., the counterion Asp-212) is located nearby the biologically active $C_{13}$=$C_{14}$ double bond[93] and, consequently, can play a role in selecting and favoring its photoisomerization (note that this structural arrangement is qualitatively similar to model **2b**). Finally, it is worth noting that in bR this anion is closer to the **N-head** than Glu-181 in Rh (which is right above the center of the unsaturated system, i.e., in a symmetric position with respect to the **N-head** and the **C-tail**). Therefore, a somehow less efficient and slower photoisomerization than that in Rh should be predicted here

(82) Conical intersections provide the outlets of the excited state paths and largely control the QYs (branching ratios) and the product manifold of the photochemical process. In PSBs these have the form of a TICT state, while in neutral linear polyenes CIs give rise to a common geometrical feature called kink (see: (a) Garavelli, M.; Bernardi, F.; Celani, P.; Robb, M. A.; Olivucci, M. *J. Photochem. Photobiol., A* **1998**, *114*, 109. (b) Fuss, W.; Haas, Y.; Zilberg, S. *Chem. Phys.* **2000**, *259*, 273. (c) Celani, P.; Garavelli, M.; Ottani, S.; Bernardi, F.; Robb, M. A.; Olivucci, M. *J. Am. Chem. Soc.* **1995**, *117*, 11584. (d) Robb, M. A.; Garavelli, M.; Olivucci, M.; Bernardi, F. *Rev. Comput. Chem.* **2000**, *15*, 87), i.e., an out of plane triangular structure that has been interpreted as a three-electron/three-center bond. Here, the three weakly coupled electrons generate a covalent-type triradicaloid fragment whose recoupling characterizes ground-state relaxation channels.
(83) Fahmy, K.; Jager, F.; Beck, M.; Zvyaga, T. A.; Sakmar, T. P.; Siebert, F. *Proc. Natl. Acad. Sci. U.S.A.* **1993**, *90*, 10206.
(84) Zhukovsky, E. A.; Oprian, D. D. *Science* **1989**, *246*, 928.
(85) Sakmar, T. P.; Franke, R. R.; Khorana, H. G. *Proc. Natl. Acad. Sci. U.S.A.* **1989**, *86*, 8309.
(86) Nakayama, T. A.; Khorana, H. G. *J. Biol. Chem.* **1991**, *266*, 4269.
(87) Mathies, R.; Stryer, L. *Proc. Natl. Acad. Sci. U.S.A.* **1976**, *73*, 2169.
(88) Johnson, R. L.; Grant, K. B.; Zankel, T. C.; Boehm, M.; Merbs, S. L.; Nathans, J.; Nakanishi, K. *Biochemistry* **1993**, *32*, 208.
(89) Nathans, J. *Biochemistry* **1990**, *29*, 9746.
(90) Ferré, N.; Olivucci, M. *J. Am. Chem. Soc.* **2003**, *125*, 6868.
(91) Ferré, N.; Cembran, A.; Garavelli, M.; Olivucci, M. *Theor. Chem. Acc.* **2004**, *112*, 335−341.
(92) Rohrig, U. F.; Guidoni, L.; Rothlisberger, U. *Biochemistry* **2002**, *41*, 10799.
(93) Edman, K.; Nollert, P.; Royant, A.; Belrhali, H.; Pebay-Peyroula, E.; Hajdu, J.; Neutze, R.; Landau, E. M. *Nature* **1999**, *401*, 822.

***Table 3.*** Computed (CASPT2/6-31G*) $S_0 \rightarrow S_1$ Vertical Absorption Energies for Model Systems **1c** and **2d** and Experimental Excitation Energies Observed (See Ref 53) for the Analogous Models **1c′** and **2d′**

| | excitation energies eV (kcal mol$^{-1}$)[98] | |
|---|---|---|
| system | computed PT2 | experimental |
| **1c** | 4.99 (115.0) | |
| **1c′** | | 3.97 (91.5)[a], 4.25 (97.9)[b] |
| **2d** | 3.94 (90.9) | |
| **2d′** | | 3.35 (77.3)[a], 3.60 (83.1)[b] |

[a] Chromophores in methylene chloride. [b] Chromophores in solid state.

(see the isomerization paths in **2a** as compared to **2b** and recall the increasing flattening of the photoisomerization channel as moving the countercharge closer to nitrogen), as in fact it has been observed.

Very remarkably, all these speculations fit the very recent experimental findings observed by Imasheva et al.[94] in proteorhodopsin (a system which is structurally similar to bR). Here, low pH protonation (i.e., neutralization) of Asp227 (the counterion residue equivalent to Asp212 in bR) leads to a drop in the QY for all-trans→13-cis photoisomerization and, concurrently, to an increase in the yield of 9-cis photoproduct formation. This is in agreement with the model of electrostatically driven catalysis presented above: in fact, neutralization of the counterion nearby the $C_{13}$═$C_{14}$ double bond is predicted to decrease its photoisomerization efficiency, which goes right in the direction observed.

Although electrostatic effects might represent only concurrent factors for the photoisomerization catalysis in the protein, still it is the first time such a contribution as been unambiguously revealed and analyzed, and we think it can be suitably exploited in the design of PSB-based artificial biomimeting photoreceptors and E→Z photoswitchable devices.

**6.5. Photoisomerization in Solution: Correlation between Computations and Observations.** Systems **1c** and **2d** qualitatively simulate an ionic pair as the one likely found in solvents[95,96] or solids (i.e., salts, matrixes, etc).[32,50,53] Therefore, **1c** and **2d** can be used as qualitative models for PSBs in condensed phase in general. Table 3 reports the calculated vertical excitation energies for these models and the experimental absorption energies recorded in condensed phase for analogous PSB systems (**1c′** and **2d′**: these have the same conjugated moiety but a different counterion).[53] Notably, although there are differences in structure and anion-type, computed values are in qualitative agreement with experiments,[98] supporting the suggestion that **1c** and **2d** are good models for ionic pairs of PSBs in condensed phase. Very remarkably, these models also provide a reasonable explanation for the less efficient and slower photoisomerization dynamics observed in solution as compared to the protein environment. In fact, in section 6.1 we have seen that **1c** and **2d** are worse photoisomerizing devices than the isolated (**1** and **2**) or **Central** (**1a**, **2a** and **2b**) systems, but we have also seen above (section 6.4) that **Central** (or isolated) models do provide a tentative first-approximation description for the chromophore into the protein binding pocket. This is particularly evident in Rh: here a symmetric displacement of three negative polar groups around the chromophore (i.e., Glu-113, Glu-181, and Glu-121; see section 6.4 and Scheme 9 above) should generate an electrostatic environment that much more resembles the situation found for the isolated or **Central** systems, where in fact very efficient barrierless photoisomerization channels (funneling the system toward TICT CI points) have been detected. Therefore, these computational results allow us to formulate a tentative and qualitative explanation for the different photoisomerization dynamics observed in solution and in the protein.

We are aware this is an oversimplification of the problem: binding pocket steric effects have been completely neglected (see also section 6.4), as well as other electrostatic interactions with more distant polar groups. Moreover, the intensity of the effect of the countercharge depends (besides its position) on its distance[99] and the type of the specific anion involved, as revealed by experimental observations for PSBs in condensed phase.[32,44,50,53] Still, we think we now have at least a qualitative picture of the reduced efficiency of the photochemical reactivity when the counterion is placed close to the **N-head** (additional results to support this point are also presented in the Supporting Information). We suggest that this electrostatic contribution might be one of the dominant components for the delayed and less efficient photoisomerizations observed in solution.

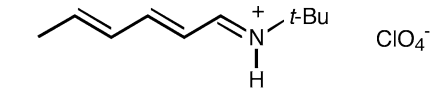


**1c'**

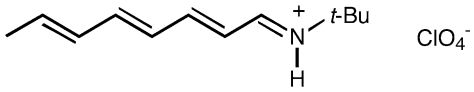


**2d'**

## 7. Conclusions

A systematic computational analysis has been presented for the position-dependent electrostatic effects of an acetate counterion on PSB photochemistry. The first task has been to provide a systematic bunch of information that might be of technological relevance and can be later on exploited for the design of artificial PSB-based photoswitchable devices. Both stereoselective and rate/efficiency effects on PSB photoisomerization have been detected, and a rationale has been presented in terms of a simple electrostatic-based model. Position and distance of the countercharge seem to be a valuable tool for tuning photoisomerization rate, efficiency, and selectivity, as well as for controlling covalent (polyene-like) vs ionic photochemistry. Speculations

(94) Imasheva, E. S.; Balashov, S. P.; Wang, J. M.; Dioumaev, A. K.; Lanyi, J. K. *Biochemistry* **2004**.
(95) Bachilo, S. M.; Bondarev, S. L.; Gillbro, T. *J. Photochem. Photobiol., B* **1996**, *34*, 39.
(96) Freedman, K. A.; Becker, R. S. *J. Am. Chem. Soc.* **1986**, *108*, 1245.
(97) Rajamani, R.; Gao, J. *J. Comput. Chem.* **2002**, *23*, 96.
(98) **2d** better agrees with experiments, possibly because in the shorter model (**1c**) appoximations are amplified due to the greater separation between the electronic states.
(99) The 3 Å distance of the counterion has been arranged according to experimental observations; see: (a) Han, M.; DeDecker, B. S.; Smith, S. O. *Biophys. J.* **1993**, *65*, 899. (b) Han, M.; Smith, S. O. *Biochemistry* **1995**, *34*, 1425. (c) Eilers, M.; Reeves, P. J.; Ying, W.; Khorana, H. G.; Smith, S. O. *Proc. Natl. Acad. Sci. U.S.A.* **1999**, *96*, 487. (d) Palczewski, K.; Kumasaka, T.; Hori, T.; Behnke, C. A.; Motoshima, H.; Fox, B. A.; Le Trong, I.; Teller, D. C.; Okada, T.; Stenkamp, R. E.; Yamamoto, M.; Miyano, M. *Science* **2000**, *289*, 739.
(100) Due to the flatness of the PES, for model **2b** the rigorous MEP has been determined only in the 0−3 au (0−2 au for model **2c**) interval. From there, a relaxed scan on the isomerizing bond has been performed, and then the distances in au have been calculated (see also the computational details).

have then been made, and a qualitative model for protein vs solution photochemistry of retinal chromophores has been presented. In particular, a computationally based explanation for the slower and less efficient dynamics observed in solution has been shown, and a new hypothesis for an electrostatically driven stereocontrolled photoisomerization in rhodopsin proteins has been suggested, which accounts for experiments and recent observations.

We think these results provide on one hand a previously lacking systematic view for photoisomerization intermolecular control by external charges and on the other a theoretical predictive reference model to compare experimental observations with. Moreover, these results may provide valuable guidelines for the tunable PSB photochemistry and for designing selective photoisomerization processes in artificial functionalized biomimetic environments. We hope this study and the predictive model presented here may stimulate new systematic experimental investigations on photoisomerization control and tuning in PSBs by countercharge environment dependent effects that can complement this computationally based view.

**Acknowledgment.** We are grateful to Prof. Buss for helpful discussions. Funds have been provided by the University of Bologna (Funds for Selected Research Topics), MIUR (funds ex 60% and project: "Stereoselezione in Sintesi Organica: Metodologie ed Applicazioni" funds ex 40%), and the FIRB project. We wish to thank CINECA for granted calculation time on their computers.

**Supporting Information Available:** Fifty-three pages containing (a) four sections (S1, S2, S3, and S4) with undocumented details and results (e.g., the results found for models **1a**, **1b**, and **1c**) plus an Appendix showing the constraints used to anchor the counterion position, (b) the Cartesian coordinates of all the structures discussed in the text, (c) two tables (Tables S1 and S2) containing the energies computed for the short models (**1a**, **1b**, and **1c**) and the details of the constraints used in the computations, respectively, and (d) the related figures and schemes (Figures S1−S6 and Scheme S1). This material is available free of charge via the Internet at http://pubs.acs.org.

JA048782+